Aerosol pH and its influencing factors in Beijing

Jing Ding[2, 1], Pusheng Zhao[1*], Jie Su[1], Qun Dong[1], Xiang Du[2, 1], and Yufen Zhang[2]

[1] Institute of Urban Meteorology, China Meteorological Administration, Beijing 100089, China

[2] State Environmental Protection Key Laboratory of Urban Ambient Air Particulate Matter Pollution Prevention and Control, College of Environmental Science and Engineering, Nankai University, Tianjin 300071, China

*** Correspondence:** P. S. Zhao (pszhao@ium.cn)

Abstract

The acidity or pH is an important feature of ambient aerosol. At present, the aerosol pH in the North China Plain, either seasonal variation or size-resolved characteristics, need to be further studied. In addition, it is also worthy of discussion about what factors have a greater impact on pH and how these factors affect pH. In view of these, the hourly water-soluble ions (SO_4^{2-}, NO_3^-, Cl^-, NH_4^+, Na^+, K^+, Mg^{2+}, and Ca^{2+}) of $PM_{2.5}$ and trace gases (HCl, HNO_3, HNO_2, SO_2, and NH_3) were online measured by a MARGA system in four seasons during 2016 and 2017 in Beijing. Furthermore, the size-resolved aerosol was also sampled by a MOUDI sampler and analyzed for the chemical compositions of different sizes. On the basis of these data, the particle hydronium ion concentration per volume air (H_{air}^+), aerosol liquid water content (ALWC), and $PM_{2.5}$ pH were calculated by using ISORROPIA-II. Moreover, the sensitivities of H_{air}^+, ALWC, aerosol pH to all the main influencing factors were discussed. In Beijing, the $PM_{2.5}$ pH over four seasons showed moderately acid. The $PM_{2.5}$ acidity in NCP was both driven by aerosol composition and particle water. The sensitivity analysis revealed that SO_4^{2-}, T, NH_4^T, and RH (only in summer) are crucial factors affecting the $PM_{2.5}$ pH. The SO_4^{2-} had a key role for aerosol acidity, especially in winter and spring. The impact of NO_3^- on $PM_{2.5}$ pH was different in four seasons. Although NH_3 in the NCP was abundant, the $PM_{2.5}$ pH was far from neutral, which mainly attributed to the limited ALWC. Elevated Ca^{2+} concentration could increase the aerosol pH because of the buffering capacity of Ca^{2+} to the acid species and the weak water solubility of $CaSO_4$. The sensitivity analysis also implied that decreasing NO_3^T could reduce the $\varepsilon(NH_4^+)$ effectively. In contrast, the nitrate response to NH_4^T control was highly nonlinear. According to the size-resolved results, the pH for coarse mode, which was near or even higher than 7, was much higher than that for fine mode. It must be noted that the aerosol pH in coarse mode showed a marked decrease when under heavily polluted condition.

Key words: Aerosol pH, ISORROPIA-II, Influencing factors, Beijing

1. Introduction

Acidity or pH, which drives many processes related to particle composition, gas-aerosol partitioning and aerosol secondary formation, is an important aerosol property (Jang et al., 2002; Eddingsaas et al., 2010; Surratt et al., 2010). The aerosol acidity has a significant effect on the aerosol secondary formation through the gas-aerosol partitioning of semi-volatile and volatile species (Pathak et al., 2011a; Guo et al., 2016). Recent studies have shown that aerosol acidity could promote the generation of secondary organic aerosol by affecting the aerosol acid-catalyzed reactions (Rengarajan et al., 2011). Moreover, metals can become soluble by acid dissociation under lower aerosol pH (Shi et al., 2011; Meskhidze et al., 2003) or by forming a ligand with organic species, such as oxalate at higher pH (Schwertmann et al., 1991). In addition, higher aerosol acidity can lower the acidification buffer capacity and affects the formation of acid rain. The investigation of aerosol acidity is conducive to better understand the important role of aerosols in acid deposition and atmospheric chemical reactions.

The hygroscopic components in the aerosols include water-soluble inorganic ions and part of organic acid (Peng, 2001; Wang et al., 2017). The deliquescence relative humidity (DRH) for the mixed-salt is lower than that of any single component (Seinfeld and Pandis, 2016), hence the ambient aerosols are generally droplets containing liquid water. The aerosol pH actually is the pH of the aerosol liquid water. The aerosol acidity is frequently estimated by the charge balance of measurable cations and anions. A net negative balance correlated with an acidic aerosol and vice versa (Zhang et al., 2007; Pathak et al., 2011b; Zhao et al., 2017). Generally, a larger value of the ion balance implies a stronger acidity or stronger alkaline. Nevertheless, an ion balance or other similar proxies fail to represent the true aerosol pH because they cannot predict H^+ concentration in the liquid phase accurately (Guo et al., 2015; Hennigan et al., 2015), which could be calculated by hydrogen ion concentration per volume air (H_{air}^+) and the aerosol liquid water content (ALWC).

It is critical to obtain the ALWC in calculating aerosol acidity. One way to calculate the ALWC is based upon the assumption that the volume of ALWC is equal to subtracting the volume of dry aerosol particles from that of wet particles (Guo et al., 2015; Bian et al. 2014; Engelhart et al. 2011). Under this assumption, ALWC could be calculated by the size-resolved hygroscopic growth factors (g(D, RH)) combining particle size distribution (PNSDs) or by the hygroscopic growth factor of

aerosol scattering coefficient (*f*(RH)) (Bian et al. 2014; Guo et al., 2015; Kuang et al., 2017a). The *g*(D, RH), defined as the ratio of the diameter of the wet particle at a certain relative humidity to the corresponding diameter at dry conditions, can be measured by a H-TDMA (Hygroscopic Tandem Differential Mobility Analyzer) (Liu et al., 1978; Swietlicki et al., 2008; Liu et al., 2011). The *f*(RH) can be observed by the wet & dry nephelometer system (Covert et al., 1972; Rood et al. 1985; Yan et al., 2009; Kuang et al., 2016, 2017b).

Another way to calculate the ALWC is based on the aerosol chemical components with thermodynamic models, such as ISORROPIA-II, AIM, ADDEM etc. (Nenes et al., 1998; Fountoukis and Nenes, 2007, Clegg et al., 1998, Topping et al., 2005a, b). Based on the aerosol chemical components as well as temperature and relative humidity, the aerosol thermodynamic models can output both ALWC and H_{air}^{+}, which offers a more precise approach to acquire aerosol pH (Pye et al., 2013). Among these thermodynamic models, ISORROPIA and ISORROPIA-II are widely used owing to its rigorous calculation and performance on computational speed. ISORROPIA simulates the gas-particle partitioning in the H_2SO_4, NH_3, HNO_3, HCl, Na^+, H_2O system, while its second version, ISORROPIA-II, adds Ca^{2+}, K^+, Mg^{2+} and the corresponding salts to the simulated particle components in thermodynamic equilibrium with water vapor and gas-phase precursors.

Comparisons were made in some studies to investigate the consistency of calculated ALWC derived from the above methods. In the North China Plain (NCP), Bian et al. (2014) found that the ALWC calculated using size-resolved hygroscopic growth factors and the PNSD agreed well with that calculated using ISORROPIA II at higher relative humidity (>60%). Relatively good consistency was also found in the study of Engelhart et al. (2011) in the USA based on the similar method. Guo et al. (2015) compared the ALWC calculated by *f* (RH) with the total predicted water by organics and inorganics. The total predicted water was highly correlated and on average within 10 % of the *f* (RH) measured water. Though good consistencies in ALWC were found among these methods, the H_{air}^{+} could only be obtained by the thermodynamic models, which had been applied to predict aerosol acidity in many studies (Nowak et al., 2006; Fountoukis et al., 2009; Weber et al., 2016; Fang et al., 2017).

The characteristics of aerosol chemical components are different among multiple size ranges.

Among inorganic ions, SO_4^{2-}, NO_3^-, Cl^-, K^+, NH_4^+ mainly concentrate in fine mode except for the dust days (Meier et al., 2009; Pan et al., 2009; Tian et al., 2014), whereas Mg^{2+}, Ca^{2+} are abundant in coarse mode (Zhao et al., 2017). The aerosol acidity is affected by coupling among many variables. Therefore, it could be expected that the aerosol pH is also diverse under different particle size. The gas precursor (NH_3, HNO_3, and HCl) of main water-soluble ions, as well as ambient temperature and relative humidity, are also important factors affecting the aerosol acidity. In some countries where particle matter concentration is very low, the pH diurnal variation was mainly driven by meteorological conditions (Guo et al., 2015, 2016; Bougiatioti et al., 2016). In China, however, the annual average $PM_{2.5}$ concentration in some megacities was ~2 times higher than the national standard value (35 μg m^{-3}) and the inorganic ions accounted for 40%~50% to $PM_{2.5}$, especially in the North China Plain (Zou et al., 2018; Huang et al., 2017; Gao et al., 2018). Hence it can be expected that the aerosol composition is also a crucial factor on pH, which cannot be ignored.

The North China Plain is the region with the most severe aerosol pollution in China. Nevertheless, only a few studies have focused on aerosol pH in this region. Some studies conducted in NCP showed that the aerosol acidity was close to neutral, while in some other studies the fine particles showed moderately acidic (Cheng et al., 2016; Wang et al., 2016; Liu et al., 2017; Shi et al., 2017). These results were all significantly higher than that in the United States or Europe, where aerosols were often highly acidic with a pH lower than 3.0 (Guo et al., 2015, 2016; Bougiatioti et al., 2016; Weber et al., 2016; Young et al., 2013). The differences in aerosol pH in NCP mainly resulted from the different methods (ion balance & thermodynamic equilibrium models) or different data sets. Moreover, the variation of $PM_{2.5}$ chemical composition in NCP in recent years also contributed to the differences in aerosol pH. The observations in previous studies exploring aerosol acidity in NCP were almost conducted before 2015. In the recent three years, the chemical composition of $PM_{2.5}$ in Beijing has undergone tremendous changes. Nitrate has replaced sulfate and is dominant in inorganic ions in most cases (Zhao et al., 2017; Huang et al., 2017; Ma et al., 2017). Moreover, studies about seasonal variation of aerosol pH and size-resolved aerosol pH are rare in NCP, and the key factors affecting aerosol acidity are still not well understood.

In this work, thermodynamic model ISORROPIA-II with the forward mode was utilized to predict ALWC and aerosol pH in Beijing. The hourly measured $PM_{2.5}$ inorganic ions and precursor

gases in four seasons during 2016 to 2017 were used to analyze the seasonal and diurnal variation of aerosol acidity, and the sensitivity analysis was conducted to identify the key factors that affecting the aerosol pH. In our previous studies, the multi-stage cascade impactors (MOUDI-122) were used for size-resolved aerosol sampling from 2013 to 2015. The actual relative humidity inside the impactors was calculated, and the size distributions of water-soluble ions, organic carbon, and elemental carbon in three seasons were discussed (Zhao et al., 2017; Su et al., 2018). Based on these size-resolved results, the pH for aerosol in different size ranges could also be predicted.

2. Data Collection and Methods

2.1 Site

The measurements were performed at the Institute of Urban Meteorology in Haidian district of Beijing (39°56'N, 116°17'E). The sampling site was located next to a high-density residential area, without significant air pollution emissions around the site. Therefore, the observation data could represent the air quality levels of the urban area of Beijing.

2.2 Online data collection

Water-soluble ions (SO_4^{2-}, NO_3^-, Cl^-, NH_4^+, Na^+, K^+, Mg^{2+}, and Ca^{2+}) of $PM_{2.5}$ and trace gases (HCl, HNO_3, HNO_2, SO_2, and NH_3) in the ambient air were measured by an online analyzer (MARGA) at hourly temporal resolution during the spring (April and May in 2016), winter (February in 2017), summer (July and August in 2017) and autumn (September and October in 2017). The more details about MARGA can be found at ten Brink et al. (2007). The $PM_{2.5}$ and PM_{10} mass concentrations (TEOM 1405DF), the hourly ambient temperature and relative humidity were also synchronously attained.

Hourly concentrations of $PM_{2.5}$, PM_{10}, and water-soluble ions in $PM_{2.5}$, as well as meteorological parameters during the observation, are shown in Figure 1. In the spring, two dust events occurred (21-22, April and 5-6, May). During the first dust events, the wind came predominantly from the north with mean wind speed 3.5 m s^{-1}. The PM_{10} concentration reached 425 μg m^{-3} while the $PM_{2.5}$ concentration was only 46 μg m^{-3} on the peak hour. Similarly, the second dust event resulted from the strong wind coming from the northwest direction. In the following pH analysis based on MARGA data, it was assumed that the particles were internally mixed, and the chemical compositions were the same for particles of different sizes in $PM_{2.5}$. Hence, these two dust events

were excluded from this analysis.

Figure 1

2.3 size-resolved chemical compositions

A Micro-Orifice Uniform Deposit Impactor (MOUDI-120) was used to collect size-resolved aerosol samples with the calibrated 50% cut sizes of 0.056, 0.10, 0.18, 0.32, 0.56, 1.0, 1.8, 3.1, 6.2, 9.9 and 18 μm. Size-resolved sampling was conducted during July 12-18, 2013; January 13-19, 2014; July 3-5, 2014; October 9-20, 2014; and January 26-28, 2015. Fifteen, fourteen, and eighteen sets of samples were obtained for the summer, autumn, and winter, respectively. Except for two sets of samples, all the samples were collected in daytime (from 08:00 to 19:00) and nighttime (from 20:00 to 7:00 the next day), respectively. One hour of preparation time was set for filter changing and nozzle plate washing with ethanol. The water-soluble ions were analyzed from the samples by using an ion chromatography (DIONEX ICS-1000). The detailed information about the features of MOUDI-120, and the procedures of sampling, pre-treatment, and laboratory chemical analysis (including the quality assurance & quality control) were described in our previous papers (Zhao et al., 2017; Su et al., 2018). It should be noted that there was no observation of gas precursors during the periods of MOUDI sampling.

2.4 Aerosol pH prediction

As mentioned in the Introduction, pH of ambient aerosols can be predicted by the thermodynamic model such as AIM and ISORROPIA. AIM is considered as an accurate benchmark model while ISORROPIA has been optimized for use in chemical transport models. Currently, ISORROPIA-II, adding K^+, Mg^{2+}, and Ca^{2+} (Fountoukis and Nenes, 2007), can calculate the equilibrium H_{air}^+ (particle hydronium ion concentration per volume air) and ALWC with reasonable accuracy by taking water-soluble ions mass concentration, temperature, and relative humidity as input. The H_{air}^+ and ALWC were then used to predict aerosol pH by the Eq. (1).

$$\mathrm{pH} = -\log_{10} H_{aq}^{+} \cong -\log_{10} \frac{1000 H_{air}^{+}}{ALWC_{i}} \quad (1)$$

Where H_{aq}^+ (mole L^{-1}) is the hydronium ion concentration in the ambient particle liquid water. H_{aq}^+ can also be deemed to be the H_{air}^+ (μg m^{-3}) divided by the concentration of ALWC associated with inorganic species, $ALWC_i$ (μg m^{-3}). Both inorganic and part of organic species in particles are

hygroscopic. However, the pH prediction is not highly sensitive to the water uptake by organic species ($ALWC_o$) (Guo et al., 2015, 2016). The similar result was also found in Beijing in Liu et al. (2017). Hence the aerosol pH could be fairly predicted by ISORROPIA-II with just measurements of inorganic species in most cases. However, it should be noted that the potential error could be incurred by ignoring $ALWC_o$ in regions where hygroscopic organic species has a relatively high contribution to fine particles.

In ISORROPIA-II, forward and reverse mode are provided to predict ALWC and H_{air}^+. In forward mode, T, RH, and the total (i.e. gas+aerosol) concentrations of NH_3, H_2SO_4, HCl, and HNO_3 need to be input. Reverse mode calculates the equilibrium partitioning given the concentrations of only aerosol compositions together with RH and T as input. In this work, the online ion chromatography MARGA was used to measure both inorganic ions of $PM_{2.5}$ and precursor gases. Moreover, several studies had shown that the ion balance and reverse-mode calculations of thermodynamic equilibrium models were not applicable to interpret the aerosol acidity (Hennigan et al., 2015; Liu et al. 2017; Song et al., 2018). The forward mode was also reported less sensitive to measurement error than the reverse mode (Hennigan et al., 2015; Song et al., 2018). Hence, ISORROPIA-II was run in the "forward mode" for aerosols in the metastable condition in this study.

When using ISORROPIA-II to calculate the $PM_{2.5}$ acidity, all particles were assumed internally mixed and the bulk properties were used, without considering the variability of chemical compositions with particle size. In the ambient atmosphere, the aerosol chemical composition is complicated, hence the deliquescent relative humidity of aerosol is generally low (Seinfeld and Pandis, 2016) and the particles usually exist in the form of droplets, which makes the assumption that the particles are in a liquid state (metastable condition) reasonable. However, when the particles are exposed to a quite low RH, the state of particles may change. Figure 2 and Figure S1-S4 exhibit the comparisons between predicted and measured NH_3, HNO_3, HCl, NH_4^+, NO_3^-, Cl^-, $\varepsilon(NH_4^+)$ ($NH_4^+/(NH_3+NH_4^+)$, mol/mol), $\varepsilon(NO_3^-)$ ($NO_3^-/(HNO_3+NO_3^-)$, mol/mol)), and $\varepsilon(Cl^-)$ ($Cl^-/(HCl+Cl^-)$, mol/mol) based on real-time ion chromatography data, which are all colored by the corresponding RH. It can be seen that agreements between predicted and measured NH_3, NH_4^+, NO_3^-, and Cl^- are pretty well, the R^2 of linear regressions are all higher than 0.94, and the slopes are around 1. Moreover, the agreement between predicted and measured $\varepsilon(NH_4^+)$ is better when compared with

206 $\varepsilon(NO_3^-)$ and $\varepsilon(Cl^-)$. The slope of linear regression between predicted and measured $\varepsilon(NH_4^+)$ was
207 0.93, 0.91, 0.95, and 0.96 and the R^2 is 0.87, 0.93, 0.89, and 0.97 in spring, winter, summer, and
208 autumn, respectively. However, measured and predicted partitioning of HNO_3 and HCl show
209 significant discrepancies (R^2 of 0.28 and 0.18), which may attribute to the much lower gas
210 concentrations compared with the particle concentrations, as well as the gas denuder measurement
211 uncertainties from particle collection artifacts (Guo et al., 2018). Obviously, more scatter points
212 deviate from the 1:1 line when ISORROPIA-II runs at RH≤30%, which is much evident in winter
213 and spring. For data with RH ≤ 30%, the predictions are significantly improved when assuming
214 aerosol in stable mode (solid + liquid) (Figure S5-S6). However, the aerosol liquid water was almost
215 zero and cannot be used to predict aerosol pH. It reveals that it is not reasonable to predict the
216 aerosol pH using the thermodynamic model when the RH is relatively low. Consequently, we only
217 discussed the $PM_{2.5}$ pH for data with RH higher than 30% in this work.

218 **Figure 2**

219 Running ISORROPIA-II in the forward mode with only aerosol concentrations as input may
220 result in a bias in predicted pH due to repartitioning of ammonia in the model, leading to a lower
221 predicted pH when gas-phase data are not available (Hennigan et al., 2015). In this work, since no
222 gas phase was available for the size-resolved pH prediction. We determined aerosol pH through an
223 iteration procedure that used the measured particulate species and ISORROPIA-II to predict gas
224 species, the detailed information could be found in Fang et al. (2017) and Guo et al. (2016). As a
225 brief summary, the predicted NH_3, HNO_3, and HCl concentrations from the *i*-1 run were applied to
226 the *i*th iteration, until the gas concentrations converged. Based on these iterative gas phase
227 concentrations, the ion concentrations from samples collected by the MOUDI as well as the
228 averaged RH and T during each sampling period were used to determine aerosol pH for different
229 size ranges. Just like calculating the pH of $PM_{2.5}$, it was also assumed that all the particles at each
230 size bin were internally mixed and had the same pH.

231 The comparisons of iterative and predicted NH_3, HNO_3, and HCl as well as measured and predicted
232 NO_3^-, NH_4^+, Cl^-, $\varepsilon(NH_4^+)$, $\varepsilon(NO_{3-})$, and $\varepsilon(Cl^-)$ for data from MOUDI samples are showed in
233 Figure 3. The previous study showed that coarse mode particles were very difficult to reach
234 equilibrium with the gaseous precursors due to kinetic limitations (Dassios et al., 1999; Cruz et al.,

2000). Assuming coarse mode particles in equilibrium with the gas phase could result in a large bias between measured and predicted NO_3^- and NH_4^+ in coarse mode particles (Fang et al, 2017). We also find that in this work, it can be clearly seen that assuming coarse mode particles in equilibrium with the gas phase could overpredict NO_3^- and Cl^- and underestimate NH_4^+ in the coarse mode (the blue scatters), which could subsequently underestimate the coarse mode aerosol pH. Compared with the coarse mode particles, the measured and predicted NO_3^-, NH_4^+, and Cl^- agreed very well in fine mode particles. Considering the kinetic limitations and nonideal gas-particle partitioning in coarse mode particles, the aerosol pH in coarse mode was determined by ignoring the gas phase.

Figure 3

2.5 Sensitivities of aerosol pH to SO_4^{2-}, NO_3^T, NH_4^T, Cl^T, RH, and T

In the real ambient air, the thermodynamic process of the aerosol is complicated, it is not easy to tell the effect of one factor on the aerosol pH. The ALWC, H_{air}^+, aerosol pH, $\varepsilon(NH_4^+)$, $\varepsilon(NO_3^-)$, and $\varepsilon(Cl^-)$ are all the output of ISORROPIA-II. Together, they reflect an objective state of particles. Considering the relative independence between input parameters, it is reasonable to discuss the influence of input variables on output parameters with the results of ISORROPIA-II. Thus, in this paper, we focus on the sensitivity analysis of single-factor variation, which can reflect the variation tendency of aerosol pH caused by the change of each variable.

In the ISORROPIA-II, the input parameters include SO_4^T (total sulfate (gas+aerosol) expressed as equivalent H_2SO_4), NO_3^T (total nitrate (gas+aerosol) expressed as equivalent HNO_3), NH_4^T (total ammonium (gas+aerosol) expressed as equivalent NH_3), Cl^T (total chloride (gas+aerosol) expressed as equivalent HCl), Na^+, Ca^{2+}, K^+, Mg^{2+}, RH, and T. After running, the gas and aerosol phase of NO_3^T, NH_4^T, and Cl^T would be reapportioned and output. In view of this, it is more reasonable to analyze the impact of NO_3^T, NH_4^T, and Cl^T on aerosol pH, rather than the impact of a single gas or aerosol phase of NO_3^T, NH_4^T, and Cl^T on aerosol pH. In addition, the mass concentration of K^+ and Mg^{2+} was low, so the variables in the sensitivity analysis were determined as SO_4^{2-}, NO_3^T, NH_4^T, Cl^T, Ca^{2+}, RH, and T. When assessing how a variable affects ALWC, H_{air}^+, and aerosol pH, the real-time measured values of this variable and the averaged values of other variables in each season were input ISORROPIA-II. The magnitude of the relative standard deviation (RSD) of calculated aerosol pH can reflect the impact of one variable on the aerosol acidity. The higher the RSD, the greater the

impact, vice versa. The average value and variation range for each variable in all four seasons are listed in Table S1 and Figure S7.

The sensitivity analysis in this work aimed at the $PM_{2.5}$ (*ie* fine particles) because the $PM_{2.5}$ components in four seasons were available and had a high temporal resolution (1h). In addition, the data set had a wide range, covering different levels of haze events. Noted that the sensitivity analysis in this work only reflected the characteristics during the observation periods, further work is needed to determine whether the sensitivity analysis is valid in other environments.

3. Results and Discussion

3.1 Overall summary of $PM_{2.5}$ pH over four seasons

The averaged $PM_{2.5}$ concentrations were 62±36, 60±69, 39±24, and 59±48 μg m^{-3} for observation periods of spring, winter, summer, and autumn, respectively (Table 1). Among all ions measured, NO_3^-, SO_4^{2-}, and NH_4^+ were three dominant species, accounting for 83% ~ 87% of total ions. Compared with other seasons, the averaged concentration of primary inorganic ions (Cl^-, Na^+, K^+, Mg^{2+}, Ca^{2+}) was higher in spring. The aerosol in Beijing showed the moderate acidity with $PM_{2.5}$ pH of 4.0±1.0, 4.5±0.7, 3.8±1.2, and 4.3±0.8 for spring, winter, summer, and autumn observation, respectively (data at RH ≤30% were excluded). The overall winter $PM_{2.5}$ pH was comparable to the result found in Beijing, 4.2 from Liu et al. (2017) and 4.5 from Guo et al. (2017), but lower than that (4.9, winter and spring) in Tianjin (Shi et al., 2017), another mega city about 120 km away from Beijing. The summer $PM_{2.5}$ pH was lowest among all four seasons. The seasonal variation of $PM_{2.5}$ pH in this work was similar to the result from Tan et al. (2018) except for spring, which was winter (4.11 ± 1.37) > autumn (3.13 ± 1.20) > spring (2.12 ± 0.72) > summer (1.82 ± 0.53). Noted that the observation in Tan et al. (2018) was conducted in Beijing in 2014, the distinction in the aerosol compositions was probably responsible for the lower $PM_{2.5}$ pH in their work.

Table 1

To further investigate the $PM_{2.5}$ pH performance under different pollution levels over four seasons, the $PM_{2.5}$ concentrations were classified into three groups with 0~75 μg m^{-3}, 75~150 μg m^{-3}, and >150 μg m^{-3}, representing the clean, polluted, and heavily polluted conditions, respectively. The relationship between $PM_{2.5}$ and its pH is shown in Figure S8. The $PM_{2.5}$ pH under clean condition spanned 2~7 while the $PM_{2.5}$ pH under polluted and heavily polluted conditions mostly concentrated

in 3~5. Table 1 shows that as the air quality deteriorated, aerosol components, as well as ALWC and H_{air}^+, all increased for each season, but the differences in $PM_{2.5}$ pH for three pollution levels were not statistically significant. In terms of the averaged values, the $PM_{2.5}$ pH under the clean condition was the highest (Table 1), then followed by polluted and heavily polluted conditions in spring, summer, and autumn. In winter, however, the averaged pH under polluted condition (4.8±1.0) was the highest, then followed by clean (4.5±0.6) and heavily polluted conditions (4.4±0.7).

Time series of mass fraction of NO_3^-, SO_4^{2-}, NH_4^+, Cl^-, and crustal ions (Mg^{2+} and Ca^{2+}) in total ions, as well as pH in all four seasons, are showed in Figure 4. It can be seen that on clean days, high $PM_{2.5}$ pH (>6) was generally companied by high mass fraction of crustal ions, while the relatively low $PM_{2.5}$ pH (<3) was companied by high mass fraction of SO_4^{2-} and low mass fraction of crustal ion, which was most obvious in summer (large part of $PM_{2.5}$ pH with RH≤30% were excluded in spring and winter). On polluted and heavily polluted days, the aerosol chemical composition was similar, mainly dominated by NO_3^-, hence the differences of $PM_{2.5}$ pH on polluted and heavily polluted days were small. Compared with the mass concentration of $PM_{2.5}$, the different aerosol chemical compositions might be the essence that drove aerosol acidity. The impact of aerosol compositions on $PM_{2.5}$ pH is discussed in Section 3.4.

Figure 4

Beijing is surrounded by mountains on three sides. Haze episodes usually occur with southwest and southeast winds as well as calm winds in Beijing. The industry is mainly concentrated in the south of Beijing, leading to the higher $PM_{2.5}$ concentration in Beijing by the regional transport and accumulation. Wind dependence of $PM_{2.5}$, NO_3^-, SO_4^{2-}, NH_4^+ and the averaged $PM_{2.5}$ pH are shown in Figure 5 and Figure S9. In spring, summer, and autumn, the $PM_{2.5}$ pH in northern direction were generally higher than that in the southwest direction, but the high pH in summer also occurred with southwest strong winds (wind speed >3 m s^{-1}). Generally, the northerly winds usually occur with cold front systems, which could sweep away air pollutants but raised dust in which the crustal ion species (Ca^{2+}, Mg^{2+}) were higher. In winter, the $PM_{2.5}$ pH distributed relatively evenly in each wind direction, but we surprisingly found that the pH in northerly winds is as low as 3~4, which was

consistent with the high mass fraction of SO_4^{2-} on the clean days caused by the northerly winds.

Figure 5

3.2 Diurnal variation of ALWC, H_{air}^+, and $PM_{2.5}$ pH

The diurnal variations of NO_3^-, SO_4^{2-}, ALWC, H_{air}^+ and $PM_{2.5}$ pH are exhibited in Figure 6. The diurnal variations for ALWC, H_{air}^+, and pH was similar over four seasons. Generally, nighttime mean ALWC was higher than daytime and reached a peak at near 04:00 ~ 06:00 (local time). After sunrise, the increasing temperatures resulted in a rapid drop in RH, leading to the obvious loss of particle water, ALWC reached the lowest level in the afternoon. H_{air}^+ was highest in the afternoon and then followed by nighttime, and H_{air}^+ was relatively low in the forenoon. The low ALWC and high H_{air}^+ resulted in the minimum pH in the afternoon. The averaged nighttime pH is 0.3~0.4 unit higher than that on daytime. Noted that the diurnal variations of $PM_{2.5}$ pH here were for the cases with RH higher than 30%. If the data at RH≤30% were included, the diurnal variations of H_{air}^+, pH, and SO_4^{2-} in winter were changed (Figure S10). H_{air}^+ and SO_4^{2-} were both higher at nighttime since the nocturnal boundary layer height was generally low in winter and easily resulted in the accumulation of SO_4^{2-}, hence leading to a lower pH at the night.

The diurnal variation of NO_3^- in winter and spring agreed well with the aerosol acidity. Nevertheless, in summer and autumn, the agreement was not well. Figure S11 shows the relationship between mass concentrations of SO_4^{2-} and NO_3^- and $PM_{2.5}$ pH at different ALWC levels for all four seasons. At the relatively low ALWC, the increasing SO_4^{2-} could decrease the pH obviously; at the relatively high ALWC, the negative correlation still existed between SO_4^{2-} mass concentration and $PM_{2.5}$ pH. On the contrary, a weak positive correlation was found between NO_3^- and pH at the relatively low ALWC and the $PM_{2.5}$ pH was almost invariable with the NO_3^- mass concentration at the relatively high ALWC. Compared with the NO_3^-, the SO_4^{2-} had a greater effect on $PM_{2.5}$ pH. When the ALWC was high enough (for example, higher than 100 μg m^{-3}), the impact of dilution of ALWC to the H_{air}^+ was more significant.

Figure 6

Guo et al. (2015) found that the ALWC diurnal variation was significant, and the diurnal pattern in pH was mainly driven by particle water dilution. However, in this work, both H_{air}^+ and ALWC had significant diurnal variations, and the aerosol acidity variation agreed well with sulfate,

indicating the aerosol acidity in NCP was both driven by aerosol composition and particle water. For example, in the winter of NCP, the $PM_{2.5}$ mass concentration in Beijing was several to dozens times higher than that in the US, which means there are more seeds in the limited particle water, and the RH was generally low, hence the dilution of aerosol liquid water to H_{air}^+ doesn't work at all, the diurnal variation of aerosol components was more important.

3.3 Gas-particle separation

Table 2 exhibits the measured $\varepsilon(NH_4^+)$, $\varepsilon(NO_3^-)$, and $\varepsilon(Cl^-)$ at different RH levels. The measured $\varepsilon(NH_4^+)$, $\varepsilon(NO_3^-)$, and $\varepsilon(Cl^-)$ increased with the elevated RH in all four seasons, indicating more NH_4^T, NO_3^T, and Cl^T were partitioned into particle phase at higher RH. In winter and spring, NO_3^T and Cl^T were dominated by particle phases, $\varepsilon(NO_3^-)$ and $\varepsilon(Cl^-)$ was higher than 65%. Whereas in summer and autumn, the lower RH generally companied by higher ambient temperature, more than half of the NO_3^T and Cl^T were partitioned into the gaseous phase. When the RH reached above 60%, more than 90% of NO_3^T and 70% of Cl^T were in the particle phase for all four seasons. Compared with $\varepsilon(NO_3^-)$ and $\varepsilon(Cl^-)$, the $\varepsilon(NH_4^+)$ was pretty lower. In spring, summer, and autumn, the average $\varepsilon(NH_4^+)$ was still lower than 0.3 even when the RH >60%, which might attribute to the higher NH_3 mass concentration in the atmosphere. The averaged NH_3 was 21.5±8.7 μg m^{-3}, 19.6±6.4 μg m^{-3}, and 16.8±8.0 μg m^{-3} in spring, summer, and autumn, respectively. In winter, the average $\varepsilon(NH_4^+)$ were much higher than that in other seasons with the relatively lower NH_3 mass concentration (4.9±2.8 μg m^{-3}).

Table 2.

3.4 Factors affecting ALWC, H_{air}^+, $PM_{2.5}$ pH, and gas-particle partitioning

As mentioned above, the aerosol chemical composition has a non-negligible effect on $PM_{2.5}$ pH. In this work, the effects of SO_4^{2-}, NO_3^T, NH_4^T, Cl^T, Ca^{2+}, RH, and T on $PM_{2.5}$ pH were performed through a sensitivity analysis over four seasons.

As shown in Table 3, for ALWC, the largest relative standard deviation (RSD) was observed when RH was taken as the evaluated factor, then followed by SO_4^{2-} or NO_3^-, which means the RH had the greatest influence on ALWC, and SO_4^{2-} and NO_3^- were major hygroscopic components in the aerosol. The SO_4^{2-}, RH, NO_3^T, and NH_4^T were all important influential factors for H_{air}^+,

especially SO_4^{2-}. The SO_4^{2-} and T were two crucial factors affecting the $PM_{2.5}$ pH variation. The $PM_{2.5}$ pH was also sensitive to NH_4^T when it was in a lower range and sensitive to RH only in summer. The relationship between pH and NH_4^T was nonlinear, the impact of NH_4^T on pH weakened as NH_4^T increased. In spring, the crucial factor for the $PM_{2.5}$ pH variation was SO_4^{2-} while it was SO_4^{2-} and NH_4^T in winter. In summer, the most important factor affecting $PM_{2.5}$ pH was RH, then followed by NH_4^T and SO_4^{2-}. In autumn, the effect of NH_4^T on $PM_{2.5}$ pH was considerable, SO_4^{2-} and T were also important. Figure 7-9 and S12-S17 show how these factors affecting the ALWC, H_{air}^+, and aerosol acidity over four seasons. The sensitivity analysis for ALWC and H_{air}^+ were similar over four seasons, while the sensitivity of $PM_{2.5}$ pH to RH and NO_3^T in four seasons were different from each other. In this study, winter and summer were chosen for a detailed discussion of sensitivity analysis because more heavy pollution episodes happened in winter while the photochemical reaction was relatively strong in summer.

Table 3

Figure 7

Figure 8

Figure 9

RH: RH had a different impact on $PM_{2.5}$ pH in different seasons. In winter, the $PM_{2.5}$ pH decreased with the increasing RH, whereas the $PM_{2.5}$ pH increased with the increasing RH in summer. In spring and autumn, the RH between 30~83% had little impact on $PM_{2.5}$ pH. The explanation for this is that the increased RH actually diluted the solution and promoted ionization, releasing H_{air}^+ and increasing ALWC as well, but the gradient was different. In winter, variation in H_{air}^+ caused by RH changes was much larger than variation in ALWC, whereas it showed an opposite tendency in summer. In autumn and spring, variation in H_{air}^+ caused by RH changes was slightly higher than the variation in ALWC. The different impact of RH on $PM_{2.5}$ pH indicated that the dilution effect of ALWC on H_{air}^+ was obvious only in summer, the high RH during the severe haze in winter could increase the aerosol acidity.

T: At high ambient temperature, $\varepsilon(NH_4^+)$, $\varepsilon(NO_3^-)$, and $\varepsilon(Cl^-)$ all showed a decreased tendency (Figure 10 and S19). The procedure of $NH_4^+ \rightarrow NH_3$ releases one H^+ to particle phase, whereas the

409 procedure of NO_3^- →HNO_3 or Cl^-→HCl both need one H^+ from the particle phase. Compared with
410 the loss of NO_3^- from NH_4NO_3 as well as Cl^- from NH_4Cl, greater loss of NH_4^+ from NH_4NO_3,
411 NH_4Cl, and $(NH_4)_2SO_4$ resulted in a net increase in particle H^+ and lower pH. In addition, the
412 molality-based equilibrium constant (H^*) of NH_3-NH_4^+ partitioning decreased faster with
413 increasing temperature when compared with that of HNO_3-NO_3^- partitioning, resulting in a net
414 increase in particle H^+ (Guo et al., 2018). Moreover, higher ambient temperature tends to lower
415 ALWC, which further decreases the $PM_{2.5}$ pH. The wide range of ambient temperature in autumn
416 made a significant impact on $PM_{2.5}$ pH in the sensitivity analysis.

417 **Figure 10**

418 **SO_4^{2-}:** SO_4^{2-} had a key role in aerosol acidity, especially in winter and spring (Figure 9, S14, S17).
419 In the sensitivity test, the $PM_{2.5}$ pH decreased by about 1.6 (4.1 to 2.5), 4.9 (5.1 to 0.2), 1.0 (3.6 to
420 2.6), and 0.9 (4.0 to 3.1) unit with SO_4^{2-} concentration went up from 0 to 40 μg m^{-3} in spring, winter,
421 summer, and autumn, respectively. In spring and winter, the ALWC was low, the variation of SO_4^{2-}
422 mass concentration could generate dramatic changes in H_{air}^+. In section 3.1, the $PM_{2.5}$ pH was lowest
423 in summer whereas highest in winter, which was consistent with the SO_4^{2-} mass faction in total ions.
424 The SO_4^{2-} mass faction in total ions in summer was highest among four seasons with 32.4%±11.1%,
425 whereas it was lowest in winter with 20.9%±4.4%.

426 **NO_3^T:** The impact of NO_3^- on $PM_{2.5}$ pH was also different, which was related to the averages of
427 input NH_4^T in different seasons. In winter, the $PM_{2.5}$ pH decreased with increasing NO_3^T
428 concentration, whereas little impact was found in summer (Figure 9). In spring and autumn, the
429 $PM_{2.5}$ pH increases first and then dropped with the increasing NO_3^T concentration (Figure S14, S17).
430 In winter, the NH_4^T mass concentration was relatively low. As NO_3^T increases, all NH_3 could be
431 converted into NH_4^+ ($\varepsilon(NH_4^+) \approx 1$). However, if HNO_3 continued to dissolve and released H_{air}^+, it
432 would result in the decrease of $PM_{2.5}$ pH. In summer, the averages of NO_3^T and Cl^T was relatively
433 low but the NH_4^T was excessive, the highest $\varepsilon(NH_4^+)$ was only 0.6 with the corresponding highest
434 NO_3^T. The excessive NH_3 could provide continuous buffering to the increasing NO_3^T, together with
435 a significant dilution of ALWC on H_{air}^+, leading to the little changes in $PM_{2.5}$ pH. In spring and
436 autumn, the increasing pH with elevated NO_3^T in lower range attributed to the dilution of ALWC to
437 H_{air}^+. H_{air}^+ concentration increased exponentially with elevated NO_3^T concentration, especially at

higher NO_3^T concentrations, whereas the ALWC increased linearly with elevated NO_3^T concentration (Figure S12-S17), hence ALWC played a dominant role when the NO_3^T concentration was low. With the further increase of NO_3^T, the variation in H_{air}^+ caused by NO_3^T addition was larger than the variation in ALWC, leading to the decrease of $PM_{2.5}$ pH. Besides, the relationship between NO_3^T and $\varepsilon(NH_4^+)$ in the sensitivity analysis showed that decreasing NO_3^T could lower the $\varepsilon(NH_4^+)$ effectively (Figure 11 and S20), which helped NH_3 maintain in the gas phase.

Figure 11

NH_4^T: The relationship between $PM_{2.5}$ pH and NH_4^T was nonlinear. NH_4^T in lower range had a significant impact on the $PM_{2.5}$ pH (Table S2), and higher NH_4^T generated limited pH change (Figure 9, S14, S17). Elevated NH_4^T could reduce H_{air}^+ exponentially and slightly increase ALWC when the other input parameters were held constant. As the NH_4^T increased, H_{air}^+ was consumed swiftly during the dissolution of NH_3 and the further reaction with SO_4^{2-}, NO_3^-, and Cl^-. The elevated NH_4^T increased the $\varepsilon(NO_3^-)$ and $\varepsilon(Cl^-)$ when NO_3^T and Cl^T were fixed (Figure 11 and S20), which means the elevated NH_4^T altered the gas-particle partition and shifted more NO_3^T and Cl^T into particle phase, leading to the deliquescence of additional nitrate and chloride and an increase of ALWC. It seems that NH_3 emission control is a good way to reduce NO_3^-. However, the relationship between NH_4^T and $\varepsilon(NO_3^-)$ in the sensitivity analysis (Figure 11 and S20) showed that the $\varepsilon(NO_3^-)$ response to NH_4^T control was highly nonlinear, which means the decrease of nitrate would happen only when the NH_4^T was greatly reduced. The same result was also obtained from a study of Guo et al (2018).

The ratio of [TA]/2[TS] provides a qualitative description for the ammonia abundance, where [TA] and [TS] are the total (gas + aqueous + solid) molar concentrations of ammonia and sulfate. The rich-ammonia is defined as [TA] > 2[TS], while if the [TA] ≤ 2[TS], then it is defined as poor-ammonia (Seinfeld and Pandis, 2016). In this work, the ratio of [TA]/2[TS] was much higher than 1 and belonged to rich-ammonia (Figure. S21). Although NH_3 in the NCP was abundant, the $PM_{2.5}$ pH was far from neutral, which might attribute to the limited ALWC. Compared to the liquid water content in clouds and precipitation, ALWC was much lower, hence the dilution of aerosol liquid water to H_{air}^+ was weak.

Cl^T: Cl^T had a relatively larger impact on the $PM_{2.5}$ pH in winter and spring compared to summer

and autumn. Except for winter, the Cl^T mass concentration was generally lower than 10 μg m^{-3}, which accounted for the little impact on $PM_{2.5}$ pH. On account of the low level of Cl^T, the dilution of ALWC on H_{air}^+ played a dominant role, generating the $PM_{2.5}$ pH increase with elevated Cl^T. However, similar to NO_3^T, higher Cl^T could decrease the $PM_{2.5}$ pH.

Ca^{2+}: In fine particles, Ca^{2+} mass concentration was generally low. In the output of ISORROPIA-II, Ca existed as $CaSO_4$ (slightly soluble). Elevated Ca^{2+} concentration could increase the $PM_{2.5}$ pH by decreasing H_{air}^+ and ALWC (Figure S18), the decreased H_{air}^+ resulted from the buffering capacity of Ca^{2+} to the acid species, while the decreased ALWC resulted from the weak water solubility of $CaSO_4$. As discussed in Section 3.1, on clean conditions, the $PM_{2.5}$ pH could reach 6~7 when the mass fraction of Ca^{2+} was high, hence the role of mineral ions on $PM_{2.5}$ pH could not be ignored in seasons (such as spring) or regions where mineral dust was an important source of fine particles. Due to the strict control measures for road dust, construction sites, and other bare ground, the nonvolatile cations in $PM_{2.5}$ decreased significantly in NCP.

3.5 Size distribution of aerosol components and pH

According to the average $PM_{2.5}$ concentration during every sampling periods, all the samples were also classified into three groups (clean, polluted, heavily polluted) with the same rule described in Section 3.1. A severe haze episode occurred during the autumn sampling, hence there were more heavily polluted samples for autumn than that in other seasons. Figure 12 shows the averaged size distributions of PM components and pH on clean, polluted, and heavily polluted conditions in summer, autumn, and winter, respectively. The NO_3^-, SO_4^{2-}, NH_4^+, Cl^-, K^+, OC, and EC mainly concentrated in the size range with aerodynamic diameters between 0.32~3.1μm, while Mg^{2+} and Ca^{2+} predominantly distributed in the coarse mode. As shown in Figure 12, the concentration levels for all chemical components increased with the increasing pollution. During the haze episodes, the sulfate and nitrate in the accumulated mode increased significantly. However, the increase of Mg^{2+} and Ca^{2+} in the coarse mode were not as obvious as secondary ions, mainly due to the low wind speed and calm atmosphere which made it more difficult to raise dust during the heavy pollution. More detailed information about size distributions of mass concentration for all analyzed species during three seasons is shown in Zhao et al. (2017) and Su et al. (2018). As mentioned in section

2.4, assuming coarse mode particles in equilibrium with the gas phase could overpredict NO_3^- and Cl^- and underestimate NH_4^+ in the coarse mode (Figure 3), which subsequently underestimated the coarse mode aerosol pH. Thus, the gas phase was ignored for pH calculation of the coarse particles (>3.1μm).

Figure 12

The aerosol pH for both fine mode and coarse mode in summer was lowest among three seasons, then followed by autumn and winter. The seasonal variation of aerosol pH derived from MOUDI data was consistent with that derived from real-time $PM_{2.5}$ chemical components measurement. In summer, the predominance of sulfate in the fine mode and high ambient temperature resulted in a low pH, ranging between 1.8 and 3.9. Aerosol pH for fine particles in autumn and winter was in the range of 2.4 ~ 6.3 and 3.5 ~ 6.5, respectively. The difference of aerosol pH between size bins in fine mode was not significant, probably owing to the excessive NH_3 (Guo et al., 2017).

As for coarse particles, the predicted pH was approximately near or even higher than 7 for all of the three seasons in this work, which mainly attributed to the buffering capacity of the coarse mode mineral dust. Simulations with extreme cases that Ca^{2+} and Mg^{2+} were removed from the input files were conducted. The results showed that the presence of Ca^{2+} and Mg^{2+} had a crucial effect on coarse mode aerosol pH (Figure S22), the difference of aerosol pH (with and without Ca^{2+} and Mg^{2+}) for particles larger than 1 μm increased with the increasing particle size. For particles smaller than 1 μm, the removal of Ca^{2+} and Mg^{2+} had little effect on aerosol pH.

The aerosol pH in coarse mode decreased significantly when under the heavily polluted condition, especially in autumn and winter. For example, the pH in stage 3 (3.1-6.2 μm) declined from 7.8 under the clean condition to 4.5 under the heavily polluted condition in winter, implying that the aerosols in coarse mode during severe hazy days would become weak acid from neutral. The obvious increase of nitrate in coarse mode might responsible for this. Moreover, the significant decrease of mass ratios of Ca^{2+} and Mg^{2+} resulted in the loss of coarse mode buffering capacity.

The size distributions of aerosol pH and all analyzed chemical components in the daytime and nighttime are illustrated in Figure S23. For summer and autumn, the pH in the nighttime was higher than that in the daytime. The diurnal variation for aerosol pH based on MOUDI data was consistent with the online data. Whereas in winter, the pH was higher in the daytime. In winter, the averaged

RH during the sampling period was relatively low, leading to a low ALWC, but the SO_4^{2-} and NO_3^- in the nighttime were obviously higher due to the lower boundary layer height. Therefore, H_{air}^+ was more abundant in nighttime while the low ALWC had little effect on pH.

5. Summary and conclusions

On the basis of online measurements, the measured and predicted NH_3, NH_4^+, NO_3^-, Cl^-, and $\varepsilon(NH_4^+)$ by using ISORROPIA-II agreed pretty well when RH was higher than 30%. It is not reasonable to assume aerosol in a liquid state (metastable) and the aerosol pH could not be accurately predicted by a thermodynamic model where the RH is relatively low. Thus, we only discussed the $PM_{2.5}$ pH for data with RH higher than 30% in this work.

In Beijing, the mean $PM_{2.5}$ pH over four seasons (RH≥30%) was 4.0±1.0 (spring), 4.5±0.7(winter), 3.8±1.2(summer), 4.3±0.8 (autumn), respectively, showing the moderate acidity. In this work, both H_{air}^+ and ALWC had significant diurnal variation, and the $PM_{2.5}$ acidity variation agreed well with sulfate, indicating the aerosol acidity in NCP was both driven by aerosol composition and particle water. The averaged nighttime pH is 0.3~0.4 unit higher than that on daytime. The $PM_{2.5}$ pH in the northerly direction was higher than that in the southwest direction.

A sensitivity analysis was performed in this work to investigate how SO_4^{2-}, NO_3^T, NH_4^T, Cl^T, Ca^{2+}, RH, and T affect ALWC, H_{air}^+, and $PM_{2.5}$ acidity. The RH affects ALWC most, then followed by SO_4^{2-} or NO_3^-. The SO_4^{2-}, RH, NO_3^T, and NH_4^T, especially SO_4^{2-}, were all important influential factors for H_{air}^+. As for $PM_{2.5}$ pH, SO_4^{2-}, T, NH_4^T, and RH (only in summer) were crucial factors.

In winter, $PM_{2.5}$ pH decreased slightly with the increasing RH, whereas the $PM_{2.5}$ pH increased with the increasing RH in summer. The dilution effect of ALWC on H_{air}^+ was obvious only in summer. In spring and autumn, the RH had little impact on $PM_{2.5}$ pH due to the comparable variations of H_{air}^+ and ALWC. The measured $\varepsilon(NH_4^+)$, $\varepsilon(NO_3^-)$, and $\varepsilon(Cl^-)$ increased with the elevated RH in all four seasons. In addition, the higher ambient temperature tended to lower $PM_{2.5}$ pH due to the volatilization of NH_4^+, NO_3^-, Cl^- and the decrease of ALWC.

SO_4^{2-} had a key role for aerosol acidity, especially in winter and spring. In spring and winter, the ALWC was relatively low, the variation of SO_4^{2-} concentration could generate dramatic changes in H_{air}^+. The impact of NO_3^- on $PM_{2.5}$ pH was different in four seasons. In winter, the $PM_{2.5}$ pH decreased with increasing NO_3^- concentration due to the low NH_4^T mass concentration. In summer,

554 the excessive NH_3 could provide continuous buffering to the increasing NO_3^T and lead to little
555 change in $PM_{2.5}$ pH.

556 The relationship between pH and NH_4^T was nonlinear, the impact of NH_4^T on $PM_{2.5}$ pH gradually
557 weakened as NH_4^T increased. Elevated NH_4^T consumed H_{air}^+ swiftly and shifted more NO_3^T and Cl^T
558 into particle phase. In NCP, NH_3 was much rich in spring, summer, and autumn, while less rich in
559 winter. Although NH_3 in the NCP was abundant, the $PM_{2.5}$ pH was far from neutral, which mainly
560 attributed to the limited ALWC.

561 Cl^T and Ca^{2+} had little impact on the $PM_{2.5}$ pH due to the low mass concentration. Elevated Ca^{2+}
562 concentration could increase the $PM_{2.5}$ pH because of the buffering capacity of Ca^{2+} to the acid
563 species and the weak water solubility of $CaSO_4$.

564 The sensitivity analysis of the relationship between NO_3^T and $\varepsilon(NH_4^+)$ imply that decreasing
565 NO_3^T could reduce the $\varepsilon(NH_4^+)$ effectively, which helped keep NH_3 in the gas phase. In contrast,
566 the nitrate response to NH_4^T control was highly nonlinear, the decrease of nitrate would happen only
567 when the NH_4^T was greatly reduced.

568 The size-resolved results showed that the pH of coarse particles was approximately near or even
569 higher than 7 for all three seasons, which was quite higher than that of fine particles. The difference
570 of aerosol pH between size bins in fine mode was not significant. The aerosol pH in coarse mode
571 decreased significantly, becoming weak acid from neutral, when under heavily polluted condition.
572 For summer and autumn, the pH in the nighttime was higher than that in the daytime. Whereas in
573 winter, the pH was higher in the daytime.

574

575 *Data availability.* All data in this work are available by contacting the corresponding author P. S.
576 Zhao (pszhao@ium.cn).

577

578 *Author contributions.* P Z designed and led this study. J D and P Z interpreted the data and discussed
579 the results. J S and X D analyzed the chemical compositions from size-resolved aerosol samples. J
580 D and P Z wrote the manuscript.

581

582 *Competing interests.* The authors declare that they have no conflict of interest.

583

584 *Acknowledgments.* This work was supported by the National Natural Science Foundation of China
585 (41675131), the Beijing Talents Fund (2014000021223ZK49), and the Beijing Natural Science
586 Foundation (8131003). Special thanks to the Max Planck Institute for Chemistry and Leibniz

587 Institute for Tropospheric Research where Dr. Zhao visited as a guest scientist in 2018.

588 ## References

589 Bian, Y. X., Zhao, C. S., Ma, N., Chen, J., Xu, W. Y.: A study of aerosol liquid water content based
590 on hygroscopicity measurements at high relative humidity in the North China Plain. Atmos. Chem.
591 Phys. 14, 6417-6426, 2014.

592 Bougiatioti, A., Nikolaou, P., Stavroulas, I., Kouvarakis, G., Weber, R., Nenes, A., Kanakidou, M.,
593 Mihalopoulos, N.: Particle water and pH in the eastern Mediterranean: Source variability and
594 implications for nutrient availability, Atmos. Chem. Phys., 16(7), 4579-4591, 2016.

595 Cheng, Y. F., Zheng, G. J., Wei C., Mu, Q., Zheng, B., Wang, Z. B., Gao, M., Zhang, Q., He, K. B.,
596 Carmichael, G., Pöschl, U., Su, H.: Reactive nitrogen chemistry in aerosol water as a source of
597 sulfate during haze events in China, Sci. Adv., 2:e1601530, 2016.

598 Clegg, S. L., et al.: A thermodynamic model of the system H^+, NH_4^+, SO_4^{2-}, NO_3^-, H_2O at
599 tropospheric temperatures, J. Phys. Chem. 102A, 2137-2154, 1998.

600 Covert, D.S., Charlson, R.J., Ahlquist, N.C.: A study of the relationship of chemical composition
601 and humidity to light scattering by aerosol. J. Appl. Meteorol. 11, 968-976, 1972.

602 Cruz, C. N., Dassios, K. G., Pandis, S. N.: The effect of dioctyl phthalate films on the ammonium
603 nitrate aerosol evaporation rate. Atmos. Environ., 34, 3897-3905, 2000.

604 Dassios, K. G., Pandis, S. N.: The mass accommodation coefficient of ammonium nitrate aerosol.
605 Atmos. Environ., 33 (18), 2993-3003, 1999.

606 Eddingsaas, N. C., VanderVelde, D. G., and Wennberg, P. O.: Kinetics and products of the acid-
607 catalyzed ring-opening of atmospherically relevant butyl epoxy alcohols, J. Phys. Chem. A, 114,
608 8106-8113, 2010.

609 Fang, T., Guo, H. Y., Zeng, L. H., Verma, V., Nenes, A., Weber, R. J.: Highly acidic ambient particles,
610 soluble metals, and oxidative potential: A link between sulfate and aerosol toxicity, Environ. Sci.
611 Technol., 51, 2611-2620, 2017.

612 Fountoukis, C., and Nenes, A.: ISORROPIA II A computationally efficient aerosol thermodynamic
613 equilibrium model for K^+, Ca^{2+}, Mg^{2+}, NH_4^+, Na^+, SO_4^{2-}, NO_3^-, Cl^-, H_2O aerosols, Atmos. Chem.
614 Phys. 7, 4639-4659, 2007.

615 Fountoukis, C., Nenes, A., Sullivan, A., Weber, R., Van Reken, T., Fischer, M., Matías, E., Moya,
616 M., Farmer, D., and Cohen, R. C.: Thermodynamic characterization of Mexico City aerosol

during MILAGRO 2006, Atmos. Chem. Phys., 9, 2141-2156, 2009.

Gao, J. J., Wang, K., Wang, Y., Liu, S. H., Zhu, C. Y., Hao, J. M., Liu, H. J., Hua, S. B., Tian, H. Z.: Temporal-spatial characteristics and source apportionment of $PM_{2.5}$ as well as its associated chemical species in the Beijing-Tianjin-Hebei region of China. Environ. Pollut., 233, 714-724, 2018.

Guo, H., Sullivan, A. P., Campuzano-Jost, P., Schroder, J. C., Lopez-Hilfiker, F. D., Dibb, J. E., Jimenez, J. L., Thornton, J. A., Brown, S. S., Nenes, A., Weber, R. J.: Fine particle pH and the partitioning of nitric acid during winter in the northeastern United States, J. Geophys. Res. Atmos., 121, 10355-10376, 2016.

Guo, H., Xu, L., Bougiatioti, A., Cerully, K. M., Capps, S. L., Hite Jr., J. R., Carlton, A. G., Lee, S.-H., Bergin, M. H., Ng, N. L., Nenes, A., Weber, R. J.: Fine-particle water and pH in the southeastern United States, Atmos. Chem. Phys., 15, 5211-5228, 2015.

Guo, H., Weber, R. J., and Nenes, A.: High levels of ammonia do not raise fine particle pH sufficiently to yield nitrogen oxide-dominated sulfate production, Sci. Rep., 7, doi: 10.1038/s41598-017-11704-0.

Guo, H., Otjes, R., Schlag, P., Scharr, A. K., Nenes, A., Weber, R. J.: Effectiveness of ammonia reduction on control of fine particle nitrate. Atmos. Chem. Phys. Discuss, https://doi.org/10.5194/acp-2018-378.

Guo, S., Hu, M., Zamor, M. L., Peng, J. F., Shang, D. J., Zheng, J., Du, Z. F., Wu, Z. J., Shao, M., Zeng, L. M., Molinac, M. J., Zhang R. Y.: Elucidating severe urban haze formation in China. PNAS, 111(49): 17373-17378, 2014.

Hennigan, C. J., Izumi, J., Sullivan, A. P., Weber, R. J., and Nenes, A.: A critical evaluation of proxy methods used to estimate the acidity of atmospheric particles, Atmos. Chem. Phys., 15, 2775-2790, 2015.

Huang, X. J., Liu, Z. R., Liu, J. Y., Hu, B., Wen, T. X., Tang, G. Q., Zhang, J. K., Wu, F. K., Ji, D. S., Wang, L. L., Wang, Y. S.: Chemical characterization and source identification of $PM_{2.5}$ at multiple sites in the Beijing–Tianjin–Hebei region, China, Atmos. Chem. Phys., 17, 12941–12962, 2017.

Jang, M., Czoschke, N. M., Lee, S., and Kamens, R. M.: Heterogeneous atmospheric aerosol

production by acidcatalyzed particle-phase reactions, Science, 298, 814-817, 2002.

Kuang, Y., Zhao, C. S., Ma, N., Liu, H. J., Bian, Y. X., Tao, J. C., and Hu, M.: Deliquescent phenomena of ambient aerosols on the North China Plain. Geophys. Res. Lett., 43, doi: 10.1002/2016GL070273, 2016.

Kuang, Y., Zhao, C. S., Zhao, G., Tao, J. C., Ma, N., and Bian, Y. X.: A novel method for calculating ambient aerosol liquid water contents based on measurements of a humidified nephelometer system. Atmos. Meas. Tech. Discuss., doi.org/10.5194/amt-2017-330, 2017a.

Kuang, Y., Zhao, C. S., Tao, J. C., Bian, Y. X., Ma, N., and Zhao, G.: A novel method for deriving the aerosol hygroscopicity parameter based only on measurements from a humidified nephelometer system. Atmos. Chem. Phys., 17, 6651–6662, 2017b.

Liu, B. Y. H., Pui, D. Y. H., Whitby, K. T., et al.: The aerosol mobility chromatograph - new detector for sulfuric-acid aerosols. Atmos. Environ., 12(1-3), 99-104, 1978.

Liu, P. F., Zhao, C. S., Göbel, T., Hallbauer, E., Nowak, A., Ran, L., Xu, W. Y., Deng, Z. Z., Ma, N., Mildenberger, K., Henning, S., Stratmann, F., and Wiedensohler, A.: Hygroscopic properties of aerosol particles at high relative humidity and their diurnal variations in the North China Plain, Atmos. Chem. Phys., 11, 3479-3494, 2011.

Liu, H. J., Zhao, C. S., Nekat, B., et al.: Aerosol hygroscopicity derived from size-segregated chemical composition and its parameterization in the North China Plain. Atmos. Chem. Phys., 14 :2525-2539, 2014.

Liu, Z., Wu, L. Y., Wang, T. H., et al.: Uptake of methacrolein into aqueous solutions of sulfuric acid and hydrogen peroxide. J. Phys. Chem. A, 116, 437-442, 2012.

Ma, Q.X., Wu, Y.F., Zhang, D. Z., Wang, X.J., Xia, Y.J., Liu, X.Y., Tian, P., Han, Z.W., Xia, X.G., Wang, Y., Zhang, R.J.: Roles of regional transport and heterogeneous reactions in the $PM_{2.5}$ increase during winter haze episodes in Beijing, Sci. Total Environ., 599-600, 246-253, 2017.

Meier, J., Wehner, B., Massling, A., Birmili, W., Nowak, A., Gnauk, T., Brüggemann, E., Herrmann, H., Min, H., Wiedensohler, A.: Hygroscopic growth of urban aerosol particles in Beijing (China) during wintertime: a comparison of three experimental methods, Atmos. Chem. Phys., 9, 6865–6880, 2009.

Meskhidze, N., Chameides, W. L., Nenes, A., and Chen, G.: Iron mobilization in mineral dust: Can anthropogenic SO_2 emissions affect ocean productivity? Geophys. Res. Lett., 30, 2085, doi:10.1029/2003gl018035, 2003.

Nenes, A., et al.: ISORROPIA: A new thermodynamic model for multiphase multicomponent inorganic aerosols, Aquatic Geochem. 4, 123-152, 1998.

Nowak, J. B., Huey, L. G., Russell, A. G., Tian, D., Neuman, J. A., Orsini, D., Sjostedt, S. J., Sullivan, A. P., Tanner, D. J., Weber, R. J., Nenes, A., Edgerton, E., Fehsenfeld, F. C.: Analysis of urban gas phase ammonia measurements from the 2002 Atlanta Aerosol Nucleation and Real-Time Characterization Experiment (ANARChE), J. Geophys. Res., 111, D17308, doi:10.1029/2006jd007113, 2006.

Pan, X. L., Yan, P., Tang, J., Ma, J. Z., Wang, Z. F., Gbaguidi, A., and Sun, Y. L.: Observational study of influence of aerosol hygroscopic growth on scattering coefficient over rural area near Beijing mega-city, Atmos. Chem. Phys., 9, 7519-7530, 2009.

Pathak, R. K., Wang, T., Ho, K. F., Lee, S. C.: Characteristics of summertime $PM_{2.5}$ organic and elemental carbon in four major Chinese cities: Implications of high acidity for water soluble organic carbon (WSOC), Atmos. Environ., 45, 318-325, 2011a.

Pathak, R. K., Wang, T. and Wu, W.S.: Nighttime enhancement of $PM_{2.5}$ nitrate in ammonia-poor atmospheric conditions in Beijing and Shanghai: Plausible contributions of heterogeneous hydrolysis of N_2O_5 and HNO_3 partitioning. Atmos. Environ., 45: 1183-1191, 2011b.

Peng, C. G., Chan, M. N., and Chan, C. K.: The hygroscopic properties of dicarboxylic and multifunctional acids: Measurements and UNIFAC predictions, Environ. Sci. Technol., 35, 4495-4501, 2001.

Pye, H. O., Pinder, R. W., Piletic, I. R., Xie, Y., Capps, S. L., Lin, Y. H., Surratt, J. D., Zhang, Z., Gold, A., Luecken, D. J., Hutzell, W. T., Jaoui, M., Offenberg, J. H., Kleindienst, T. E., Lewandowski, M., and Edney, E. O.: Epoxide pathways improve model predictions of isoprene markers and reveal key role of acidity in aerosol formation, Environ. Sci. Technol., 47, 11056-11064, 2013.

Rengarajan, R., Sudheer, A.K., Sarin, M.M.: Aerosol acidity and secondary formation during wintertime over urban environment in western India. Atmos. Environ., 45: 1940-1945, 2011.

Rood, M.J., Larson, T.V., Covert, D.S., Ahlquist, N.C.: Measurement of laboratory and ambient aerosols with temperature and humidity controlled nephelometry. Atmos. Environ. 19, 1181-1190, 1985.

Schwertmann, U., Cornell, R. M.: Iron Oxides In the Laboratory: Preparation and Characterization,

Weinheim, WCH Publisher, 1991.

Seinfeld, J. H., Pandis, S. N.: Atmospheric Chemistry and Physics: From Air Pollution to Climate Change, John Wiley & Sons, Inc., Hoboken, New Jersey, USA, 2016.

Shi, G. L., Xu, J., Peng, X., Xiao, Z. M., Chen, K., Tian, Y. Z., Guan, X. P., Feng, Y. C., Yu, H. F., Nenes, A., Russell, A. G.: pH of aerosols in a polluted atmosphere: source contributions to highly acidic aerosol, Environ. Sci. Technol., DOI: 10.1021/acs.est.6b05736, 2017.

Shi, Z., Bonneville, S., Krom, M. D., Carslaw, K. S., Jickells, T. D., Baker, A. R., Benning, L. G.: Iron dissolution kinetics of mineral dust at low pH during simulated atmospheric processing. Atmos. Chem. Phys., 11, 995-1007, 2011.

Song, S. J., Gao, M., Xu, W. Q., Shao, J. Y., Shi, G. L., Wang, S. X., Wang, Y. X., Sun, Y. L., McElroy, M. B.: Fine particle pH for Beijing winter haze as inferred from different thermodynamic equilibrium models. Atmos. Chem. Phys., 18, 7423-7438, 2018.

Su, J., Zhao, P. S., Dong, Q.: Chemical Compositions and Liquid Water Content of Size-Resolved Aerosol in Beijing. Aerosol Air Qual. Res., 18, 680-692, 2018.

Surratt, J. D., Chan, A. W., Eddingsaas, N. C., Chan, M., Loza, C. L., Kwan, A. J., Hersey, S. P., Flagan, R. C., Wennberg, P. O., and Seinfeld, J. H.: Reactive intermediates revealed in secondary organic aerosol formation from isoprene, P. Natl. Acad. Sci. USA, 107, 6640-6645, 2010.

Swietlicki, E., Hansson, H.-C., Hämeri, K., Svenningsson, B., Massling, A., McFiggans, G., McMurry, P.H., Petäjä, T., Tunved, P., Gysel, M., Topping, D., Weingartner, E., Baltensperger, U., Rissler, J., Wiedensohler, A., Kulmala, M.: Hygroscopic properties of submicrometer atmospheric aerosol particles measured with H-TDMA instruments in various environments: a review. Tellus Ser. B Chem. Phys. Meteorol. 60, 432-469, 2008.

Tan, T. Y., Hu, M., Li, M. R., Guo, Q. F., Wu, Y. S., Fang, X., Gu, F. T., Wang, Y., Wu, Z. J.: New insight into $PM_{2.5}$ pollution patterns in Beijing based on one-year measurement of chemical compositions. Sci. Total Environ., 621, 734-743, 2018.

ten Brink, H., Otjes, R., Jongejan, P., Slanina, S.: An instrument for semicontinuous monitoring of the size-distribution of nitrate, ammonium, sulphate and chloride in aerosol. Atmos. Environ. 41, 2768-2779, 2007.

Tian, S. L., Pan, Y. P., Liu, Z.R., Wen, T. X., Wang, Y. S.: Size-resolved aerosol chemical analysis of extreme haze pollution events during early 2013 in urban Beijing, China. J.

737 Hazard. Mater., 279, 452-460, 2014.
738 Topping, D. O., McFiggans, G. B., and Coe, H.: A curved multicomponent aerosol hygroscopicity
739 model framework: Part 1– Inorganic compounds, Atmos. Chem. Phys., 5, 1205-1222, 2005a.
740 Topping, D. O., McFiggans, G. B., and Coe, H.: A curved multicomponent aerosol hygroscopicity
741 model framework: Part 2 – Including organic compounds, Atmos. Chem. Phys., 5, 1223-1242,
742 2005b
743 Wang, G., Zhang, R., Gomez, M. E., Yang, L., Levy Zamora, M., Hu, M., Lin, Y., Peng, J., Guo, S.,
744 Meng, J., Li, J., Cheng, C., Hu, T., Ren, Y., Wang, Y., Gao, J., Cao, J., An, Z., Zhou, W., Li, G.,
745 Wang, J., Tian, P., Marrero-Ortiz, W., Secrest, J., Du, Z., Zheng, J., Shang, D., Zeng, L., Shao,
746 M., Wang, W., Huang, Y., Wang, Y., Zhu, Y., Li, Y., Hu, J., Pan, B., Cai, L., Cheng, Y., Ji, Y.,
747 Zhang, F., Rosenfeld, D., Liss, P. S., Duce, R. A., Kolb, C. E., and Molina, M. J.: Persistent sulfate
748 formation from London Fog to Chinese haze, Proc. Natl. Acad. Sci. U.S.A., 113, 13630-13635,
749 2016.
750 Wang, X. W., Jing, B., Tan, F., Ma, J.B., Zhang, Y. H., Ge, M.F.: Hygroscopic behavior and chemical
751 composition evolution of internally mixed aerosols composed of oxalic acid and ammonium
752 sulfate, Atmos. Chem. Phys., 17, 12797-12812, 2017.
753 Weber, R. J., Guo, H., Russell, A. G., Nenes, A.: High aerosol acidity despite declining atmospheric
754 sulfate concentrations over the past 15 years. Nat. Geosci., 9, 282-285, 2016.
755 Yan, P., Pan, X., Tang, J., et al.: Hygroscopic growth of aerosol scattering coefficient: A comparative
756 analysis between urban and suburban sites at winter in Beijing. Particuology, 7, 52-60, 2009.
757 Young, A. H., Keene, W. C., Pszenny, A. A. P., Sander, R., Thornton, J. A., Riedel, T. P., Maben, J.
758 R.: Phase partitioning of soluble trace gases with size-resolved aerosols in near-surface
759 continental air over northern Colorado, USA, during winter, J. Geophys. Res. Atmos., 118, 9414-
760 9427, doi:10.1002/jgrd.50655, 2013.
761 Zhang, Q., Jimenez, J. L., Worsnop, D. R., Canagaratna, M.: A case study of urban particle acidity
762 and its influence on secondary organic aerosol. Environ. Sci. Technol., 41, 3213-3219, 2007.
763 Zhao, P. S., Chen, Y. N., Su, J.: Size-resolved carbonaceous components and water-soluble ions
764 measurements of ambient aerosol in Beijing. J. Environ. Sci., 54, 298-313, 2017.
765 Zhao, P. S., Dong, F., He, D., Zhao, X.J., Zhang, X.L., Zhang, W.Z., Yao, Q., Liu, H. Y.:
766 Characteristics of concentrations and chemical compositions for $PM_{2.5}$ in the region of Beijing,

767 Tianjin, and Hebei, China. Atmos. Chem. Phys., 13, 4631-4644, 2013.
768 Zou, J. N., Liu, Z. R., Hu, B., Huang, X. J., Wen, T. X., Ji, D. S., Liu, J. Y., Yang, Y., Yao, Q., Wang,
769 Y. S.: Aerosol chemical compositions in the North China Plain and the impact on the visibility in
770 Beijing and Tianjin. Atmos. Res. 201, 235-246, 2018.

Table captions

Table 1. Average mass concentrations of NO_3^-, SO_4^{2-}, NH_4^+ and $PM_{2.5}$ as well as RH, ALWC, H_{air}^+, and $PM_{2.5}$ pH under clean, polluted, and heavily polluted conditions over four seasons.

Table 2. Average $\varepsilon(NH_4^+)$, $\varepsilon(NO_3^-)$, $\varepsilon(Cl^-)$, and ambient temperature at different ambient RH levels in four seasons.

Table 3. Sensitivity of ALWC, H_{air}^+, and $PM_{2.5}$ pH to SO_4^{2-}, NH_4^T, NO_3^T, Cl^T, Ca^{2+}, RH, and T. The larger magnitude of the relative standard deviation (RSD) represents the larger impact derived from the variation of variables.

.

Table 1

Spring	$PM_{2.5}$	NO_3^-	SO_4^{2-}	NH_4^+	ALWC*	H_{air}^{+*}	pH*
	μg m^{-3}	μg m^{-3}	μg m^{-3}	μg m^{-3}	μg m^{-3}	μg m^{-3}	
Average	62±36	14.9±14.6	9.7±7.9	7.9±7.3	23±35	6.8E-06±2.8E-05	4.0±1.0
Clean	44±17	7.9±6.6	6.2±3.7	4.8±3.2	14±26	3.2E-06±5.1E-06	4.1±1.1
Polluted	100±21	30.8±14.3	16.4±5.9	15.4±5.8	33±36	5.1E-06±4.3E-06	3.9±0.5
Heavily polluted	169±12	45.3±8.5	36.3±4.9	29.4±2.3	78±60	2.0E-05±6.5E-06	3.6±0.3
Winter	$PM_{2.5}$	NO_3^-	SO_4^{2-}	NH_4^+	ALWC*	H_{air}^{+*}	pH*
Average	60±69	13.7±21.0	7.3±8.7	7.3±10.0	35±46	2.2E-05±2.3E-04	4.5±0.7
Clean	22±20	3.6±3.9	2.8±1.8	2.2±2.0	10±16	3.2E-07±4.8E-07	4.5±0.6
Polluted	107±21	18.9±8.6	11.0±5.7	11.0±4.7	41±45	1.9E-05±9.1E-05	4.8±1.0
Heavily polluted	209±39	59.7±21.8	26.2±6.3	29.1±8.7	80±52	7.0E-05±4.7E-04	4.4±0.7
Summer	$PM_{2.5}$	NO_3^-	SO_4^{2-}	NH_4^+	ALWC*	H_{air}^{+*}	pH*
Average	39±24	9.5±9.5	8.6±7.5	7.2±5.6	50±68	1.6E-05±1.8E-05	3.8±1.2
Clean	33±18	7.3±6.8	7.0±6.0	5.9±4.0	42±61	1.4E-05±1.6E-05	3.8±1.2
Polluted	87±13	26.5±10.5	20.7±7.0	17.6±4.8	100±88	3.1E-05±2.0E-05	3.5±0.4
Autumn	$PM_{2.5}$	NO_3^-	SO_4^{2-}	NH_4^+	ALWC*	H_{air}^{+*}	pH*
Average	59±48	18.5±19.5	6.5±5.9	8.2±8.2	109±160	8.1E-06±1.1E-05	4.3±0.8
Clean	33±21	7.6±7.4	4.4±4.1	3.8±3.5	49±83	3.8E-06±6.6E-06	4.5±1.0
Polluted	105±21	33.8±11.6	14.3±6.3	16.0±4.6	225±189	1.7E-05±1.2E-05	4.1±0.3
Heavily polluted	174±18	63.4±15.4	25.0±15.9	29.0±5.1	317±236	2.2E-05±1.0E-05	4.1±0.2

* For data with RH>30%.

792 **Table 2**

793

	RH	T, ℃	ε(NH_4^+)	ε(NO_3^-)	ε(Cl^-)
Spring	⩽ 30 %	24.8 ± 3.7	0.17±0.14	0.84±0.12	0.67±0.24
	30~60 %	20.6 ± 3.8	0.25±0.14	0.91±0.06	0.82±0.16
	>60 %	15.8 ± 2.7	0.28±0.12	0.96±0.03	0.96±0.06
Winter	⩽ 30 %	5.4 ± 5.3	0.31±0.13	0.78±0.12	0.89±0.14
	30~60 %	1.0 ± 3.6	0.50±0.21	0.89±0.10	0.97±0.03
	>60 %	-1.9 ± 2.1	0.60±0.20	0.96±0.03	0.99±0.01
Summer	⩽ 30 %	35.6± 0.4	0.06±0.02	0.35±0.20	0.39±0.17
	30~60 %	29.6 ± 4.2	0.17±0.11	0.65±0.23	0.43±0.16
	>60 %	25.2 ± 3.8	0.26±0.12	0.90±0.12	0.71±0.15
Autumn	⩽ 30 %	21.7± 7.5	0.07±0.06	0.49±0.25	0.45±0.21
	30~60 %	20.8± 6.3	0.21±0.14	0.82±0.19	0.67±0.21
	>60 %	14.9 ± 5.7	0.30±0.19	0.92±0.10	0.86±0.13

794

795

Table 3

Impact Factor		SO_4^{2-}	NO_3^T	NH_4^T	Cl^T	Ca^{2+}	RH	T
Spring	RSD-ALWC	50.5%	53.4%	2.9%	7.5%	21.2%	122%	13.1%
	RSD-H_{air}^+	223%	34.4%	26.8%	12.4%	49.8%	115%	49.5%
	RSD-pH	**12.4%**	5.2%	3.9%	2.4%	5.5%	1.3%	7.0%
Winter	RSD-ALWC	33.8%	28.7%	14.2%	30.7%	1.9%	103%	3.5%
	RSD-H_{air}^+	431%	431%	187.4%	52.3%	11.3%	136%	74.1%
	RSD-pH	**28.1%**	8.4%	**27.0%**	3.8%	1.0%	4.1%	6.7%
Summer	RSD-ALWC	49.4%	46.0%	6.9%	3.6%	9.0%	104%	10.8%
	RSD-H_{air}^+	131%	29.9%	78.1%	3.4%	18.1%	44.6%	33.9%
	RSD-pH	**7.9%**	3.6%	**8.1%**	0.8%	1.9%	**8.6%**	5.8%
Autumn	RSD-ALWC	32.8%	58.1%	9.9%	6.9%	3.3%	77.6%	5.5%
	RSD-H_{air}^+	171%	126.7%	333.1%	2.0%	9.3%	106%	59.6%
	RSD-pH	**6.0%**	3.3%	**16.1%**	1.0%	0.8%	2.4%	**7.5%**

Figure captions

Figure 1. Time series of relative humidity (RH), temperature (T) (a, e, i, m); $PM_{2.5}$, PM_{10}, and NH_3 (b, f, g, n); dominant water-soluble ion species: NO_3^-, SO_4^{2-}, and NH_4^+ (c, g, k, o); and $PM_{2.5}$ pH colored by $PM_{2.5}$ concentration (d, h, l, p) over four seasons.

Figure 2. Comparisons of predicted and measured NH_3, HNO_3, HCl, NH_4^+, NO_3^-, Cl^-, $\varepsilon(NH_4^+)$, $\varepsilon(NO_3^-)$, and $\varepsilon(Cl^-)$ colored by RH. In this Figure, the data of four seasons were put together, and the comparisons for each season were shown in Figure S1-S4.

Figure 3. Comparisons of predicted and iterative NH_3, HNO_3, and HCl, as well as the predicted and measured NH_4^+, NO_3^-, Cl^-, $\varepsilon(NH_4^+)$, $\varepsilon(NO_3^-)$, and $\varepsilon(Cl^-)$ colored by particle size. In this Figure, all MOUDI data were put together.

Figure 4. Time series of mass fraction of NO_3^-, SO_4^{2-}, NH_4^+, Cl^-, and crustal ions (Mg^{2+}, Ca^{2+}) in total ions as well as $PM_{2.5}$ pH in all four seasons.

Figure 5. Wind dependence map of $PM_{2.5}$ pH over four seasons. In each picture, the shaded contour indicates the average of variables for varying wind speeds (radial direction) and wind directions (transverse direction).

Figure 6. Diurnal patterns of mass concentrations of NO_3^- and SO_4^{2-} in $PM_{2.5}$, predicted aerosol liquid water content (ALWC), H_{air}^+, and $PM_{2.5}$ pH over four seasons. Mean and median values are shown, together with 25% and 75 % quantiles. Data with RH≤30% were excluded, the shadow represents the time period when the RH lower than 30% mostly occurred.

Figure 7. Sensitivities of H_{air}^+ to SO_4^{2-}, NO_3^T, NH_4^T, and Cl^T, as well as meteorological parameters (RH, T) in summer and winter.

Figure 8. Sensitivities of ALWC to SO_4^{2-}, NO_3^T, NH_4^T, and Cl^T, as well as meteorological parameters (RH, T) in summer and winter.

Figure 9. Sensitivities of $PM_{2.5}$ pH to SO_4^{2-}, NO_3^T, NH_4^T, and Cl^T, as well as meteorological parameters (RH, T) in summer and winter.

Figure 10. Sensitivities of $\varepsilon(NH_4^+)$, $\varepsilon(NO_3^-)$, and $\varepsilon(Cl^-)$ to NO_3^T, NH_4^T, and Cl^T colored by $PM_{2.5}$ pH in summer and winter.

Figure 11. Sensitivities of $\varepsilon(NH_4^+)$, $\varepsilon(NO_3^-)$, and $\varepsilon(Cl^-)$ to RH and T colored by $PM_{2.5}$ pH in summer and winter.

Figure 12. The size distributions of aerosol pH and all analyzed chemical components under clean (a, d, g), polluted (b, e, h), and heavily polluted conditions (c, f, i) in summer, autumn, and winter.

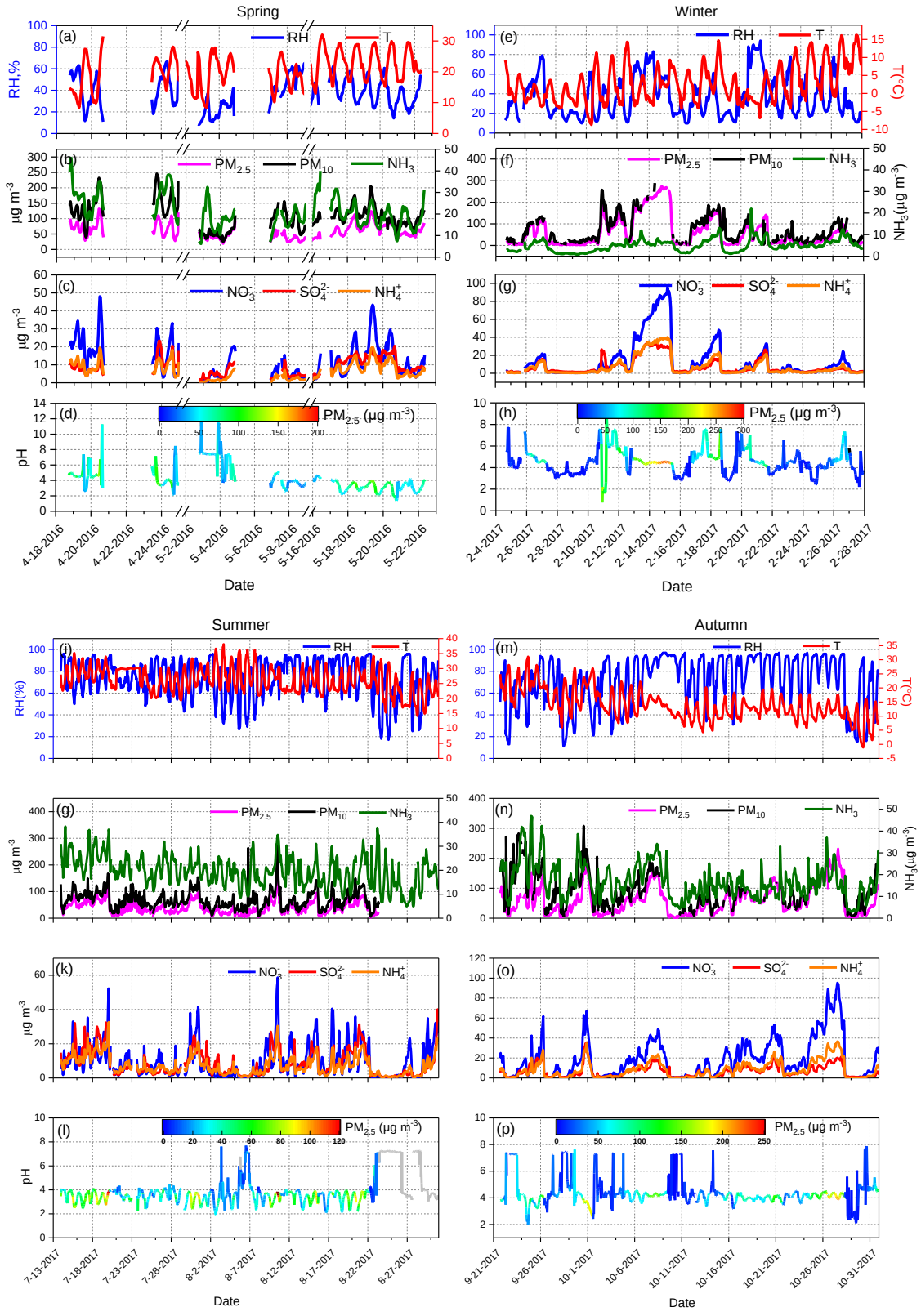
Spring
Winter
Summer
Autumn
RH
T
PM2.5
PM10
NH3
NO3-
SO42-
NH4+
RH,%
T(°C)
μg m-3
NH3(μg m-3)
pH
PM2.5 (μg m-3)
Date

Figure 1.

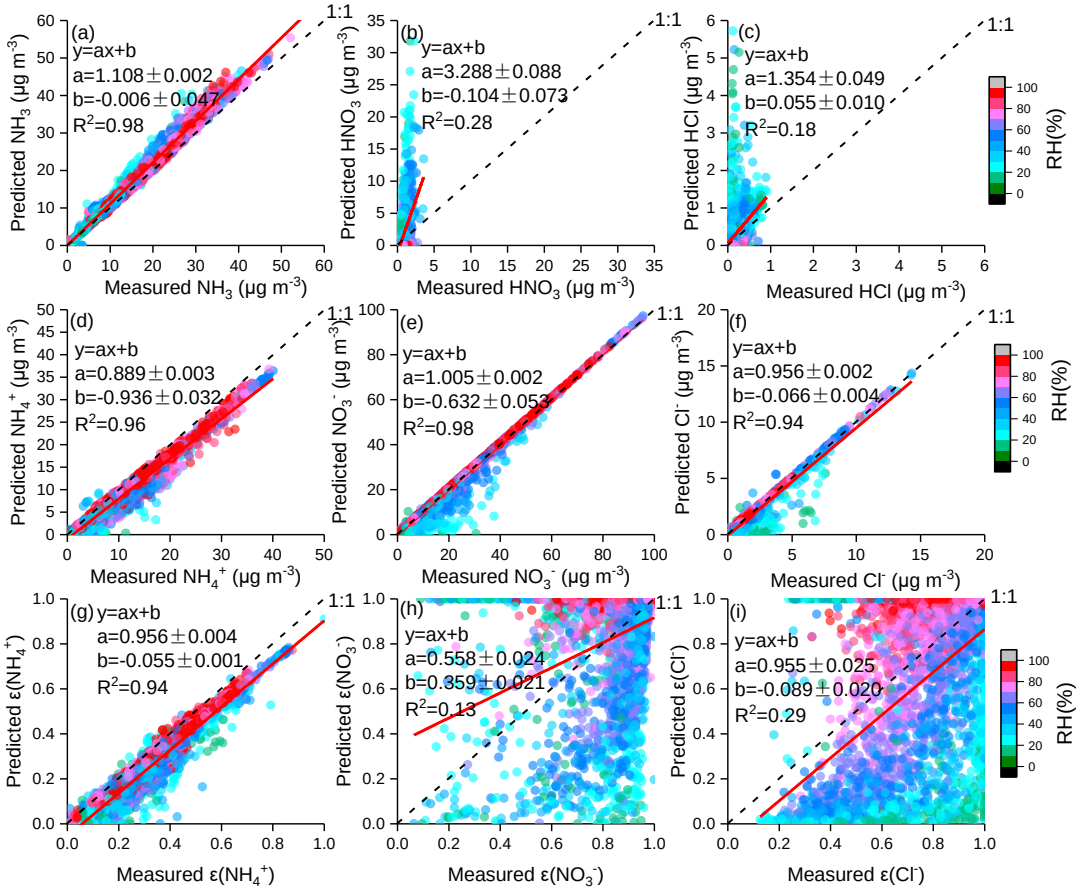
(a)
y=ax+b
a=1.108±0.002
b=-0.006±0.047
R²=0.98
Predicted NH3 (μg m-3)
Measured NH3 (μg m-3)
(b)
y=ax+b
a=3.288±0.088
b=-0.104±0.073
R²=0.28
Predicted HNO3 (μg m-3)
Measured HNO3 (μg m-3)
(c)
y=ax+b
a=1.354±0.049
b=0.055±0.010
R²=0.18
Predicted HCl (μg m-3)
Measured HCl (μg m-3)
RH(%)
(d)
y=ax+b
a=0.889±0.003
b=-0.936±0.032
R²=0.96
Predicted NH4+ (μg m-3)
Measured NH4+ (μg m-3)
(e)
y=ax+b
a=1.005±0.002
b=-0.632±0.053
R²=0.98
Predicted NO3- (μg m-3)
Measured NO3- (μg m-3)
(f)
y=ax+b
a=0.956±0.002
b=-0.066±0.004
R²=0.94
Predicted Cl- (μg m-3)
Measured Cl- (μg m-3)
RH(%)
(g)
y=ax+b
a=0.956±0.004
b=-0.055±0.001
R²=0.94
Predicted ε(NH4+)
Measured ε(NH4+)
(h)
y=ax+b
a=0.558±0.024
b=0.359±0.021
R²=0.13
Predicted ε(NO3-)
Measured ε(NO3-)
(i)
y=ax+b
a=0.955±0.025
b=-0.089±0.020
R²=0.29
Predicted ε(Cl-)
Measured ε(Cl-)
RH(%)
1:1

Figure 2.

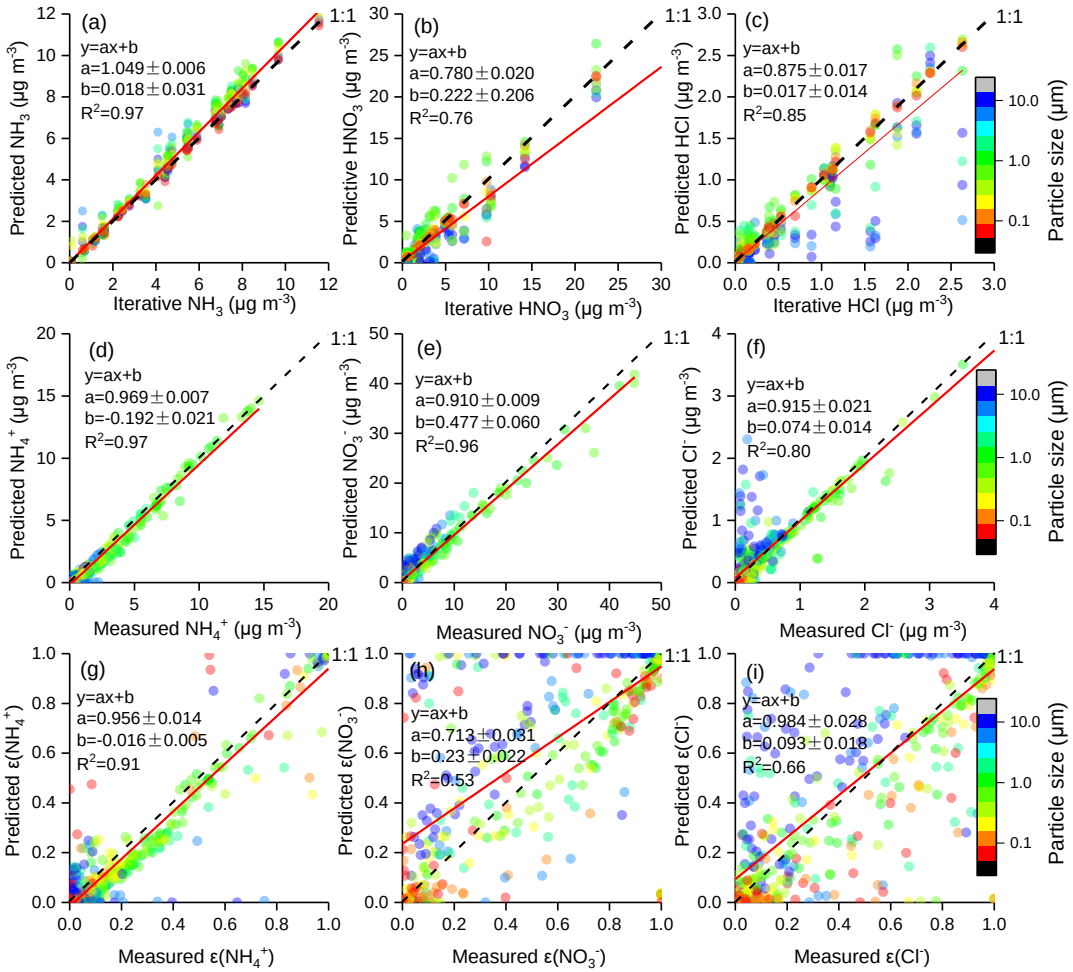

840

841 **Figure 3.**

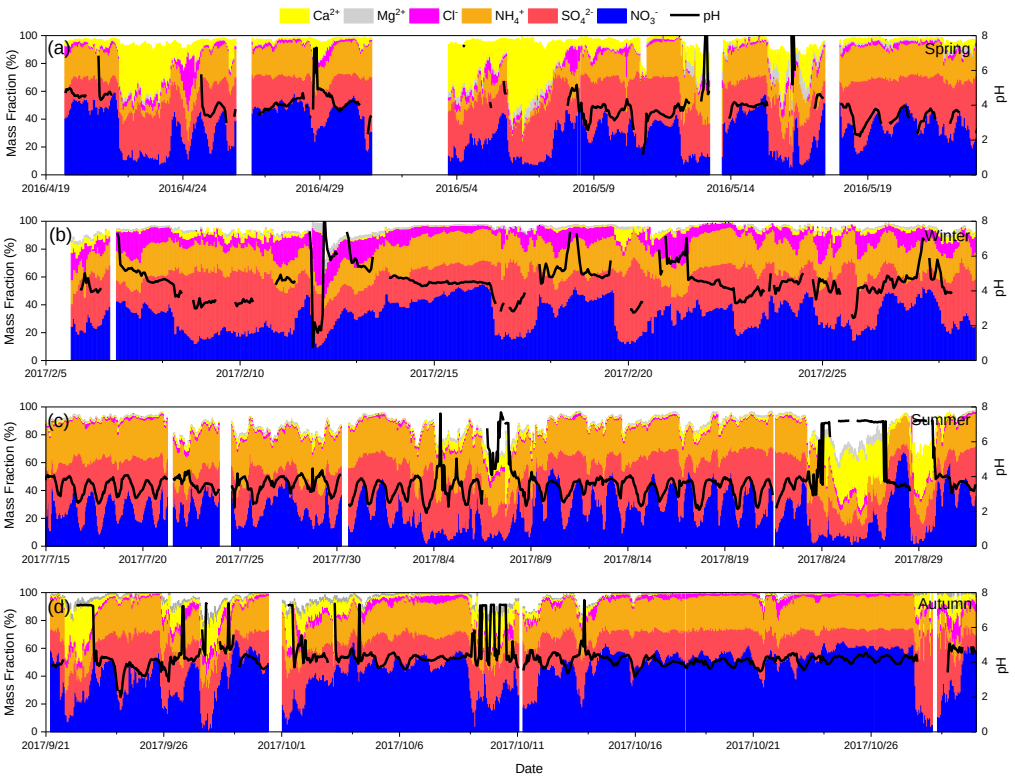

Figure 4.

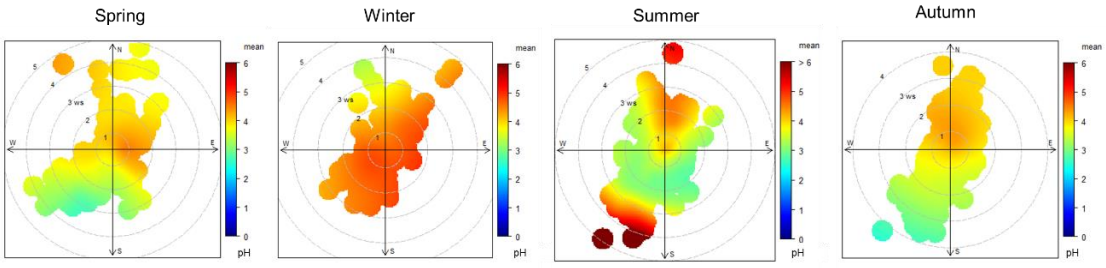

Figure 5.

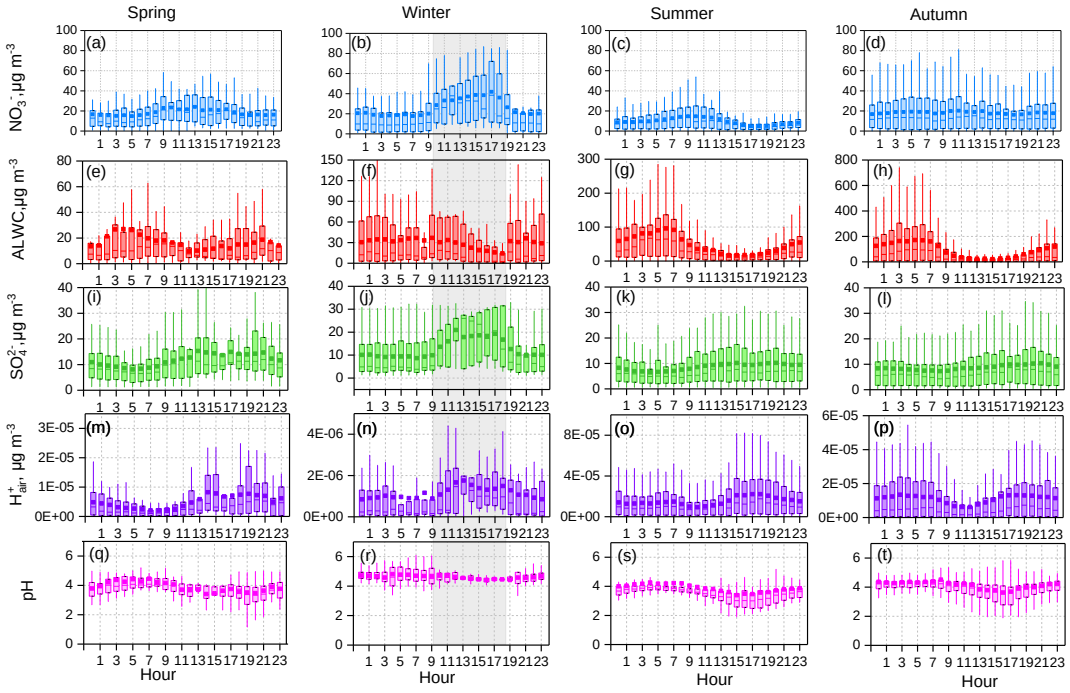

Figure 6.

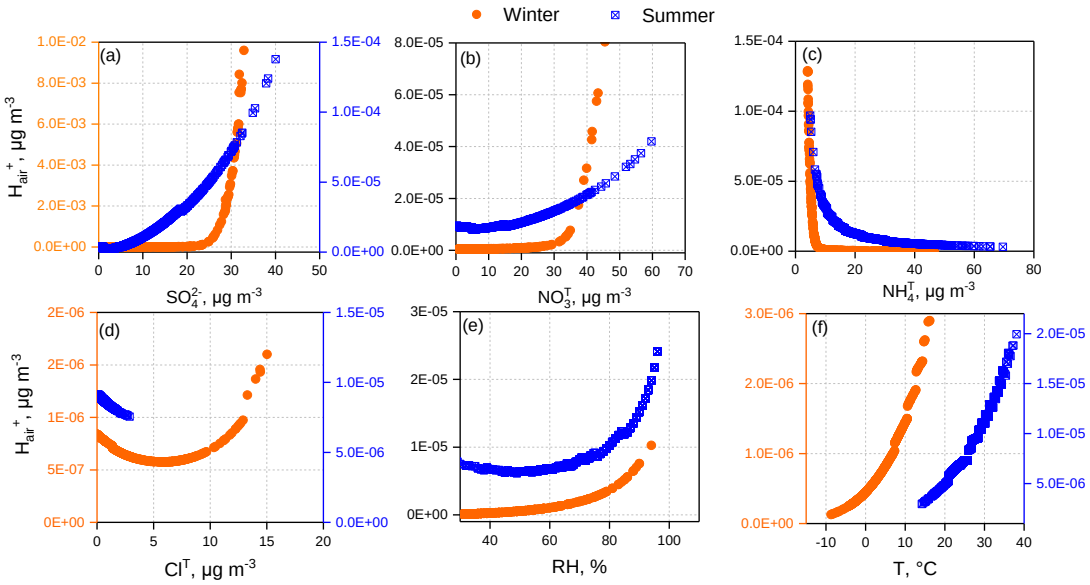

Figure 7.

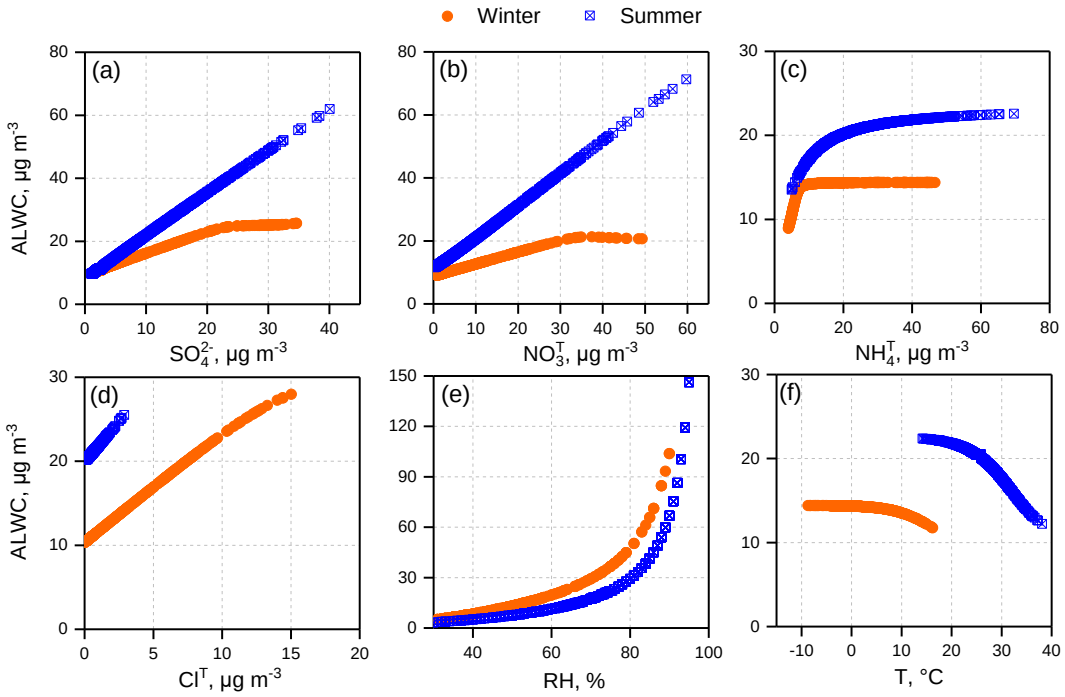

865

866 **Figure 8.**

867

868

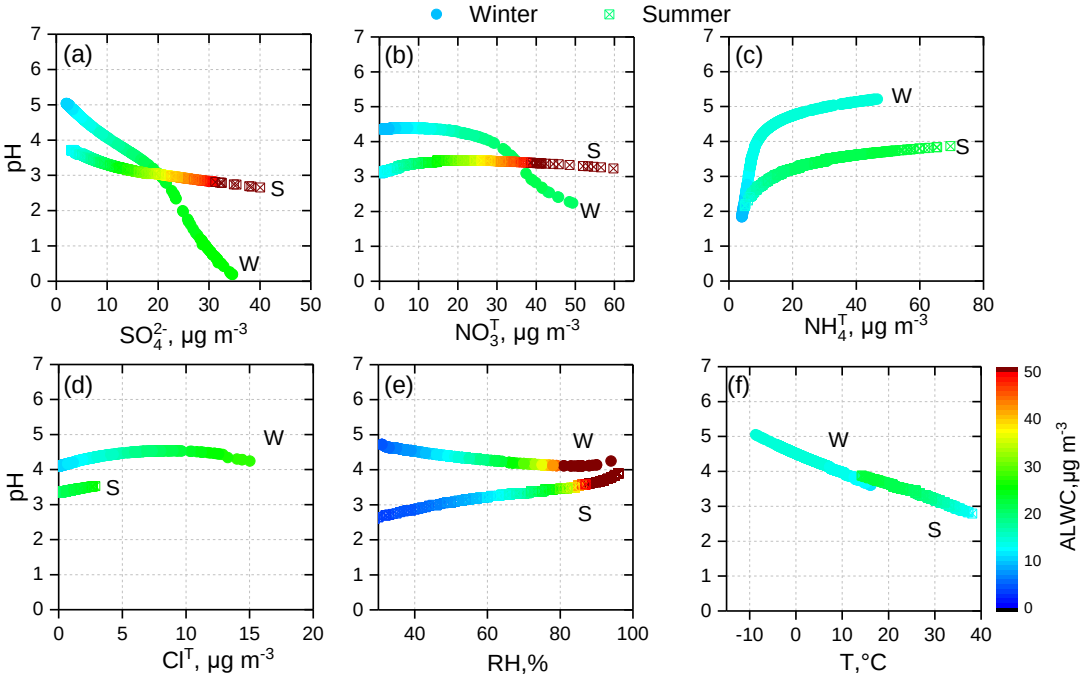

869

870 **Figure 9.**

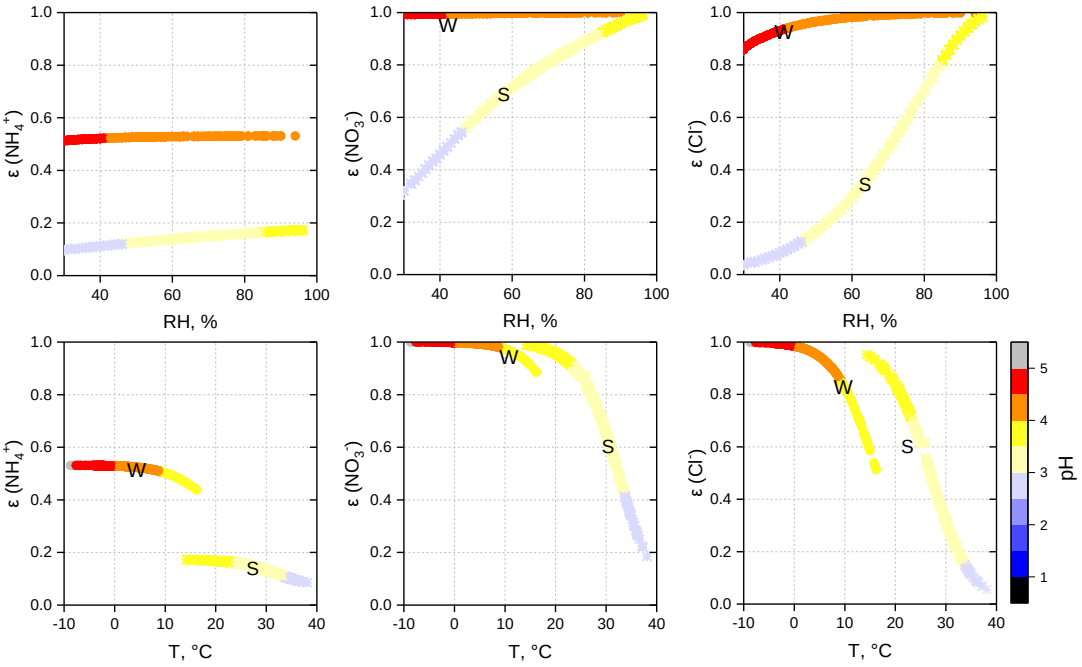

871

872 **Figure 10.**

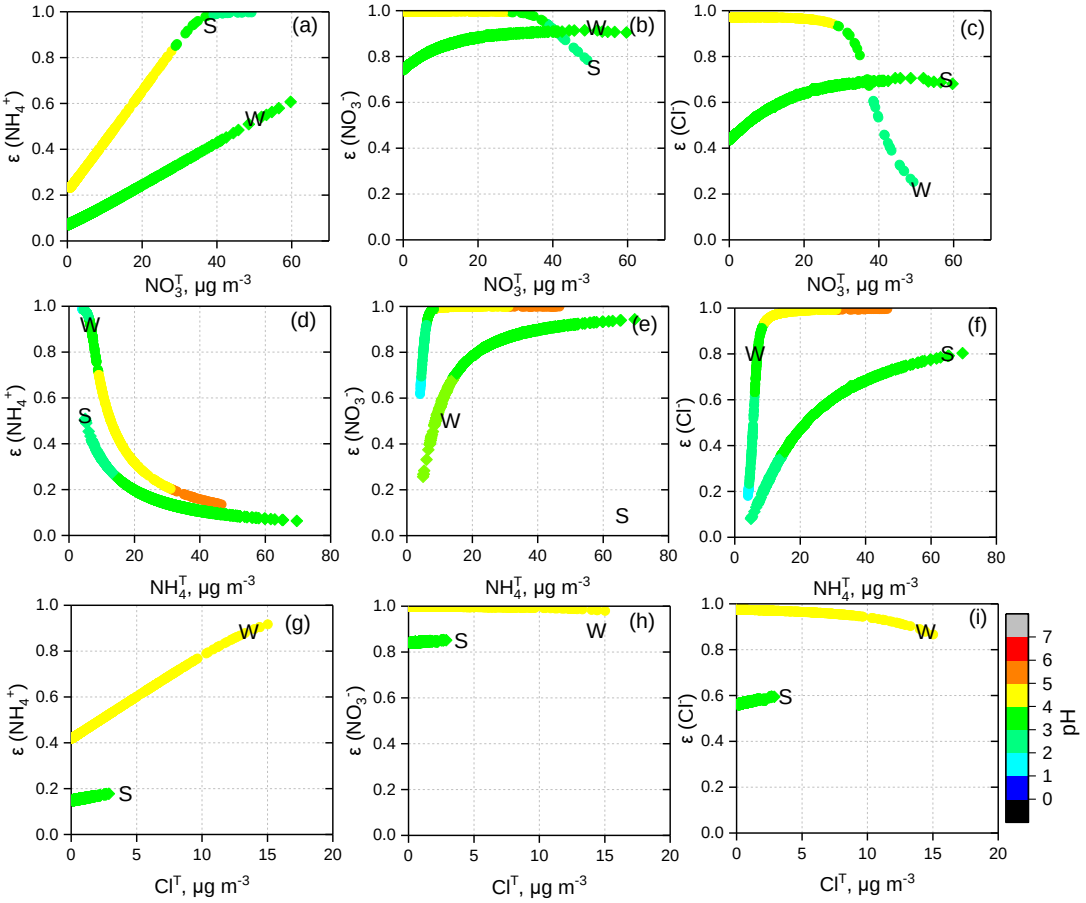

873
874

875 **Figure 11.**

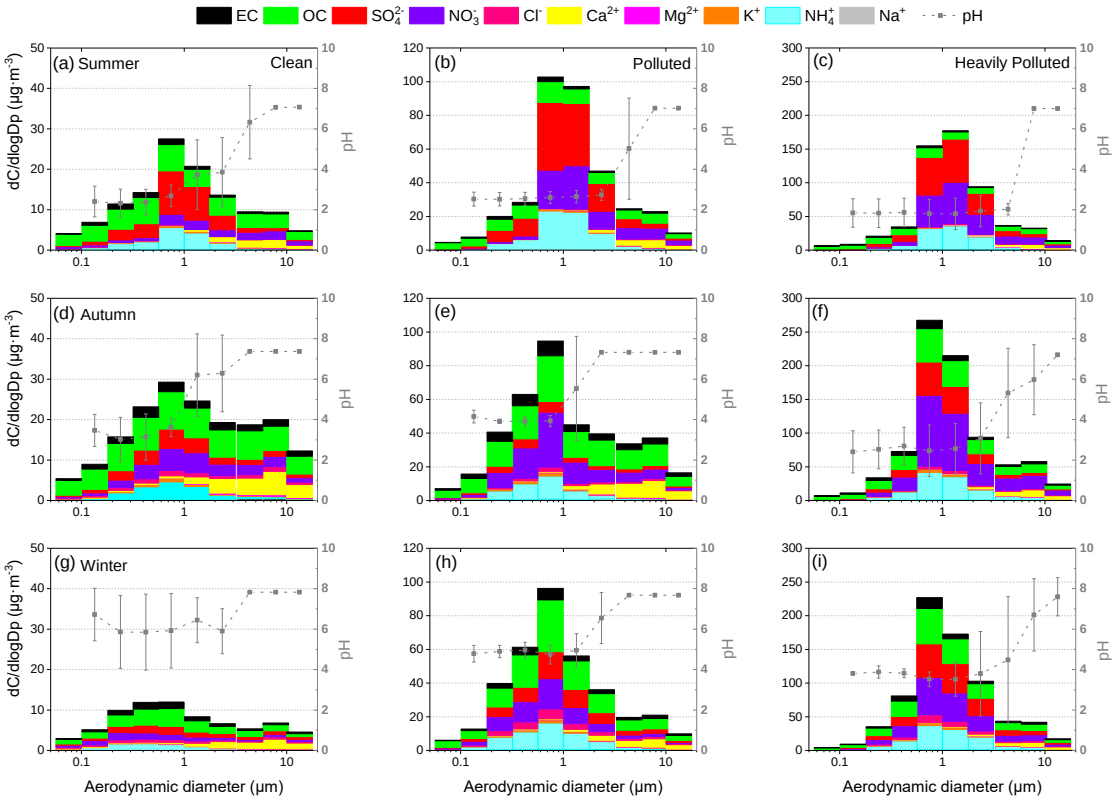
EC
OC
SO_4^{2-}
NO_3^-
Cl^-
Ca^{2+}
Mg^{2+}
K^+
NH_4^+
Na^+
pH
(a) Summer
Clean
(b)
Polluted
(c)
Heavily Polluted
(d) Autumn
(e)
(f)
(g) Winter
(h)
(i)
dC/dlogDp (μg·m^{-3})
pH
Aerodynamic diameter (μm)

Figure 12.